An analytic model to study the radiative and thermodynamical properties of a corona around a compact object

Jesse Roomer
Engineering physics

July 5, 2022

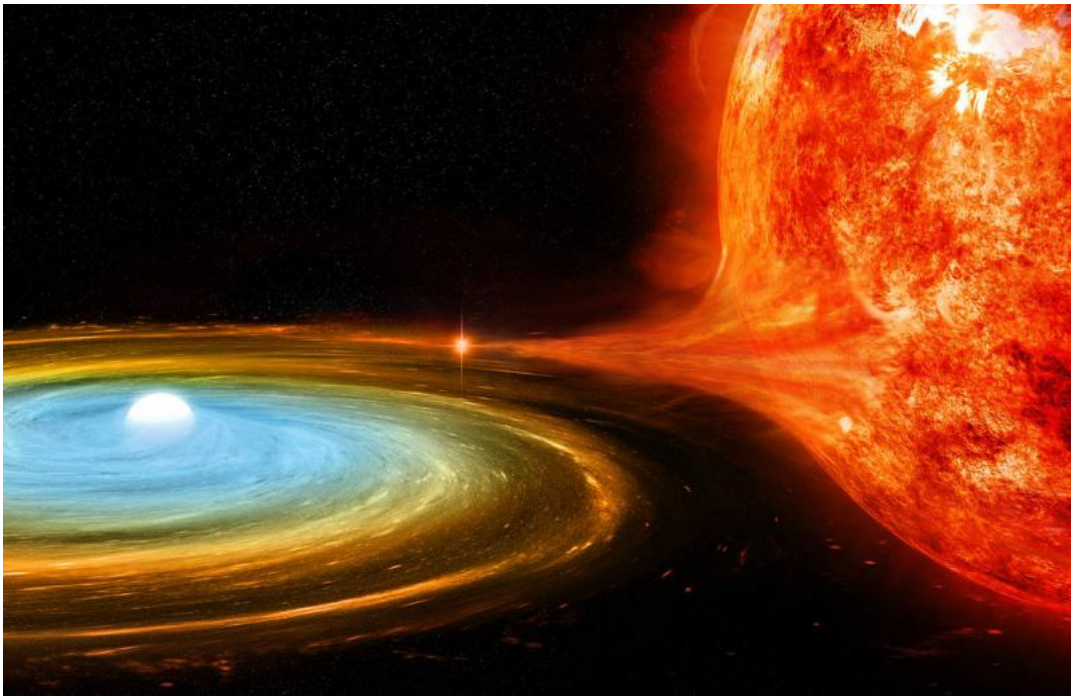

An analytic model to study the radiative and thermodynamical properties of a corona around a compact object

Author:	Jesse Roomer
Time period:	September 2020 - January 2021
Organisation:	Kapteyn Astronomical Institute, University of Groningen
Department:	Faculty of Science and Engineering
Place and country:	Groningen, The Netherlands
Supervisors at Kapteyn:	Prof. Dr. R.M. Mendez and Dr. F. Garcia
Supervisor at Fontys:	Dr. Urs Wyder

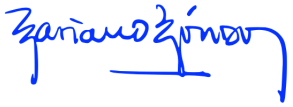

Approved:

Prof. Dr. Mariano Mendez
Date: January 10, 2021

Cover image: Compact object accretion. From: https://chandra.harvard.edu/blog/node/701

Samenvatting

In een binair systeem met een ster en een compact object (zwart gat, neutronen ster of witte dwerg) wordt massa overgedragen van de ster naar het compacte object. Deze massa vormt een accretieschijf rondom het compacte object en er onstaat ook een zogeheten corona waarin zich elektronen bevinden. Deze elektronen kunnen botsen met de fotonen in de schijf en hierdoor worden de fotonen verstrooid naar hogere energieën. Dit zorgt ervoor dat de elektronen energie verliezen in wat inverse-Compton verstrooiing wordt genoemd.
Een model dat de verdeling van de fotonen die de corona verlaten beschrijft als een functie van tijd en energie is gecreëerd door Becker [5]. Dit model bevat aannames die het model minder nauwkeurig maken. Een van deze aannames is dat de bron niet zal veranderen in temperatuur en een constante fotoninjectiesnelheid geeft. Het doel was om een op Python gebaseerd computermodel te maken om een realistischer model te verkrijgen. Dit nieuwe model bevat temperatuur en fotoninjectie variaties.

Becker [5] verkrijgt een exacte gesloten-vorm expressie voor de tijdsafhankelijke oplossing van de Green's functie voor de Kompaneets'-vergelijking. De Kompaneets'-vergelijking beschrijft de spectrale modificatie van een fotondistributie als deze door een hete elektronenpopulatie beweegt. [19] De Green's functie kan worden gebruikt om differentiaalvergelijkingen op te lossen, zoals de Kompaneets'-vergelijking.[10] De verkregen oplossing beschrijft de evolutie in de energieruimte van een fotondistributie die in eerste instantie mono-energetisch is. De oplossing is gecodeerd in een Python model en grafieken zijn gegenereerd om deze te vergelijken met de grafieken uit Becker [5]. Hieruit blijkt dat de grafieken uit het Python-model en uit de publicatie van Becker [5] identiek zijn, waarmee is aangetoond dat het Python-model correct is.

Twee eigenschappen van de Green's functie worden onderzocht. De gemiddelde fotonenergie en de inverse-Compton temperatuur zijn aan het Python-model toegevoegd en de resultaten worden afgebeeld in figuren. Deze resultaten worden vergeleken met de figuren van Becker's publicatie [5] en het blijkt dat ze hetzelfde zijn.

De tijdsafhankelijke fotonenergie-verdeling voor een bremsstrahlung beginspectrum is berekend en uitgezet in de publicatie door Becker [5]. Hetzelfde is gedaan voor het gecreëerde Python-model en de grafiek die ontstaat wordt vergeleken met de grafiek uit de publicatie. Omdat ze nagenoeg identiek zijn, wordt de fotonenergie-verdeling voor een initieel spectrum van een zwarte straler toegevoegd aan het Python-model als uitbreiding op Becker zijn publicatie [5]. Hiervoor is gekozen voor een zwarte straler omdat dit spectrum meer het werkelijke spectrum van een compact object weergeeft. [9, 15]

De tijdsafhankelijke ontsnappingsfoton-verdeling in consante eenheden van de ontsnappingstijd en in constante eenheden van de injectiesnelheid worden ook aan het Python-model toegevoegd. Becker [5] heeft dit gedaan voor een mono-energetisch initieel spectrum voor beide gevallen. Ook heeft hij dit gedaan voor een bremsstrahlung initieel spectrum voor de tijdsafhankelijke ontsnappingsfoton-verdeling in eenheden van de ontsnappingstijd. Het gecreëerde Python-model genereerd dezelfde grafieken als in de publicatie van Becker [5]. Daarnaast is er ook een initieel spectrum van een zwarte straler voor beide gevallen toegevoegd.

De tijdsafhankelijke ontsnappingsfoton-verdeling in eenheden van de injectiesnelheid met een variërende injectiesnelheid wordt aan het Python-model toegevoegd voor een initieel spectrum van een zwarte straler. Hier varieert de injectiesnelheid sinusoïdaal, terwijl de temperatuur constant wordt gehouden. Het Python-model zal de spectra, lichtcurven en frequenctiespectra teruggeven. In de spectra van het Python-model is ook een schuifregelaar over de tijd toegevoegd

om de veranderingen van het spectrum over de tijd weer te geven.
Tot slot is de tijdsafhankelijke ontsnappingsfoton-verdeling in eenheden van de injectiesnelheid met een variërende temperatuur van de zwarte straler opgenomen. Hier wordt de temperatuur van de zwarte straler sinusoïdaal gevarieerd, terwijl de injectiesnelheid constant wordt gehouden. Het model genereert de lichtcurven, spectra en frequenctiespectra van de ontsnappingsfoton-verdeling voor de genoemde temperatuur variaties.
Een aanbeveling op het model en eventuele volgende stappen worden besproken. Er worden aanbevelingen gedaan om de effectiviteit van het model te verbeteren en om het model realistischer te maken.

Summary

In a binary system containing a star and compact object (black hole, neutron star, or white dwarf) mass is transferred from the star to the compact object. This mass will form an accretion disc around the compact object and will also form a so-called corona which contains electrons. These electrons can interact with photons in the disc, as a result, the photons can be up-scattered to higher energies. This will cause the electrons to lose energy in what is called Inverse-Compton scattering.
A model describing the distribution of photons leaving the corona as a function of time and energy has been created by Becker [5]. This model includes assumptions that make it less accurate. One of the assumptions is that the source will not change in temperature and inputs a constant photon injection rate. The goal was to create a Python-based computer model to obtain a more realistic model. This new model includes temperature and photon injection variations.

Becker [5] obtains an exact closed-form expression for the time-dependent Green's function solution to the Kompaneets' equation. The Kompaneets' equation describes the spectral modification of a photon distribution as it moves through a hot electron population. [19] Green's functions can be used to solve differential equations such as the Kompaneets' equation. [10] The solution obtained describes the evolution in energy space of a photon distribution that is initially mono-energetic. This solution is coded into the Python-model and plotted to compare with the figure from Becker [5], and it is found that they are identical.

Two properties of the Green's function are explored: The mean photon energy and inverse-Compton temperature are inserted into the Python-model and the results are plotted. These results are compared with the figures from Becker's paper [5] and it is found that they are the same.

The time-dependent photon energy distribution for a bremsstrahlung initial spectrum is found and plotted in the paper by Becker [5]. The same is done for the Python-model created and the graph that arises is compared with the graph from the paper. Seeing they are similar, the photon energy distribution for a blackbody initial spectrum is added to the Python-model as an extension to the paper by Becker [5]. This is done because the spectrum of a compact object resembles that of a blackbody. [9, 15]

The time-dependent escaping photon distribution in units of the escape time and in units of the constant injection rate are also added to the Python-model. Becker [5] has done this for a mono-energetic initial spectrum for both cases. He also did this for a bremsstrahlung initial spectrum in units of the escape time.
The escaping photon distributions for a mono-energetic initial spectrum in units of the escape time and in units of the injection rate from the Python-model are identical to the figures in Becker's paper [5] and therefore it can be said that the Python-model works. Then a blackbody initial spectrum is added in the model for the escaping photon distribution.

The time-dependent escaping photon distribution in units of the injection rate with a varying injection rate is added to the Python-model for a blackbody initial spectrum. Here the injection rate varies sinusoidal, while the temperature is kept constant. The Python-model will return the spectra, light curves, and power spectra. A slider over time in the spectra is also added in the model to explore the changes in the spectrum over time.
Finally, the time-dependent escaping photon distribution in units of the injection rate with a varying blackbody temperature is included in the Python-model. Here the temperature of the blackbody is varied sinusoidally while the injection rate is kept constant. The model generates the light curves, spectra, and power spectra for this varying temperature.

A recommendation for the model and possible next steps are discussed in this report. Here recommendations to improve the efficiency of the model and recommendations to create a more realistic model are included.

Foreword

The Kapteyn Astronomical Institute is a research institute for astronomy. It is an institute of the faculty of Science and Engineering of the University of Groningen and has been named after the founder of the institute: Jacobus Cornelius Kapteyn.
The Kapteyn Institute focuses on four research topics which are connected to the NOVA network (NW). These topics are Galaxy structure, Formation and Evolution (NW1), Interstellar Medium and Star and Planet Formation (NW2), Cosmology and Large Scale Structure (NW1), High-Energy Astrophysics and Active Galaxies (NW1, NW3). Another research field is advanced instrumentation and Data Science and Virtual Observatories. [2]

This report obtains a model to study the radiative and thermodynamical properties of a corona around a compact object. Here the spectra, light curves and power spectra of the time-dependent escaping photon distribution are obtained for a continuous and varying injection rate, but also for a varying source temperature with continuous injection rate.

The project is supervised by Prof. Dr. Mariano Mendez of Kapteyn Institute and his post-doctoral fellow Dr. Federico Garcia of the Kapteyn Institute and Urs Wyder of Fontys University of Applied Sciences. I would like to thank them for their help and support in supervising me on this internship. I learned a lot from them and their way of explaining things to me. They were very patient when I did not understand things and were more than willing to explain everything. Also a special thanks to Prof. Dr. Mariano Mendez for giving me the opportunity to graduate at the Kapteyn Institute. I would like to thank the University of Groningen and last but not least I would like to thank Valentina Peirano who occasionally helped me with my research.

Used abbreviations

- FFT: Fast Fourier Transform
- LMXB: Low Mass X-ray Binary
- HMXB: High Mass X-ray Binary
- kHz QPO: Kilohertz Quasi Periodic Oscillations

Used symbols (cgs units)

- x: energy [-]
- x_0: initial energy [-]
- y: Compton y-parameter/dimensionless time [-]
- n_e: electron number density $[cm^{-3}]$
- σ_T: Thomson cross section $[cm^2]$
- c: speed of light $[cm/s]$
- kT_e: Electron temperature $[keV]$
- m_e: electron mass $[g]$
- t: time $[s]$
- t_0: initial time $[s]$
- x_*: critical energy [-]
- T_{eff}: effective temperature of radiation $[K]$
- P: escape time distribution [-]
- N_r: number of photons in the cloud at time t [-]
- N_0: number of photons injected in the cloud at time $t = t_0$ [-]
- t_{esc}: mean escape time of a photon $[s]$
- N_x: number of photons in the cloud at time t with energy between x and $x + dx$ [-]
- A: amplitude [-]
- ω: angular frequency $[rad/s]$

Contents

1. Introduction

In a binary system containing a star and compact object (black hole, neutron star, or white dwarf) mass is transferred from the star to the compact object. This mass will form an accretion disc around the compact object and will also form a so-called corona which contains electrons. These electrons can interact with photons from the disc, as a result, the photons can be up-scattered to higher energies. This will cause the electrons to lose energy in what is called Inverse-Compton scattering.
A model describing the distribution of photons leaving the corona as a function of time and energy has been created by Becker [5]. This model includes assumptions that make it less accurate. One of the assumptions is that the corona will not change in temperature and the source that injects photons into the corona has a constant photon injection rate. The goal is to create a more realistic model by including temperature and photon injection variations.

Becker [5] obtains an exact closed-form expression for the time-dependent Green's function solution to the Kompaneets' equation. The Kompaneets' equation describes the spectral modification of a photon distribution as it moves through a hot electron population. [19] Green's function can be used to solve differential equations such as the Kompaneets' equation.[10] The solution obtained describes the evolution in energy space of a photon distribution that is initially mono-energetic.[5] The theory behind this will be described in section 2.
Before implementing variations into the mathematical model created by Becker [5], the model has to be coded into a Python-based computer model. In section 3 the graphs of the computer model are compared with the graphs from the paper to verify whether the computer model works. Becker [5] only creates graphs for a mono-energetic initial spectrum or bremsstrahlung initial spectrum. In addition to what was presented in Becker's paper, the computer model created also includes a blackbody initial spectrum. The reason for this is that a spectrum of a compact object resembles a blackbody initial spectrum. [9, 15] The results for this are shown in section 3.1 to 3.6. Further on, a temperature and photon injection rate variation is added to obtain an even more realistic model. This is shown in sections 3.7 and 3.8. The Fast Fourier Transform (FFT) can be performed on these results to obtain the power spectra of the escaping photon distribution as can be seen in sections 3.7 and 3.8.
Finally section 4 will give a discussion on the results obtained from the model and section 5 and section 6 will respectively obtain a conclusion to the goal set here and give some recommendations for the model.

2. Theoretical background

2.1. Analytical time-dependent Green's function solution to the Kompaneets' equation

Compton-scattering occurs between photons and electrons in a hot, radiation-dominated plasma. Appendix A.3 provides further information about Compton-scattering and Appendix A.4 about binary systems where the corona is created. This scattering, also called Comptonisation, alters the X-ray spectra and Fast Fourier Transform (FFT) of the light curves. The time lags and power-law tails that are seen in X-ray spectra are the results of thermal Comptonisation. This thermal Comptonisation is described by the Kompaneets' equation given by equation (40) in Appendix A.5. The Kompaneets' equation describes the effects of energy diffusion, electron recoil, and spatial diffusion. Energy diffusion is the change of energy of the photons with time and spatial diffusion is the diffusion of photons from one place to another. Including the electron recoil will include the energy that is transferred (lost or gained) by the photons when interacting with the electrons. Becker [5] derived the time-dependent Green's function for an infinite, homogeneous plasma with steady properties using the Kompaneets' equation, where the Green's function is used to solve partial differential equations. Appendix A.6 explains Green's functions in more detail. The solution will include the effect of electron recoil and diffusion of photons in the energy space. Because these effects are included, the equation will approach the Wien spectrum given by equation (39) at large values of the time. Appendix A.2 can be addressed for further information about the Wien's law. Spatial diffusion is not included here since the cloud is infinite and the diffusion will be added later when a finite cloud is assumed. The Green's function solution describes the evolution in energy space of a photon distribution that is initially mono-energetic and is given by [5]

$$f_G(x, x_0, y) = \frac{32}{\pi} e^{-9y/4} x_0^{-2} x^{-2} e^{(x_0-x)/2} \int_0^\infty e^{-u^2 y} \frac{u \sinh(\pi u)}{(1+4u^2)(9+4u^2)} W_{2,iu}(x_0) W_{2,iu}(x)\, du + \frac{e^{-x}}{2} + \frac{e^{-x-2y}}{2} \frac{(2-x)(2-x_0)}{x_0 x}. \tag{1}$$

Here y is the dimensionless time or Compton-y parameter given by

$$y(t) \equiv n_e \sigma_T c \frac{kT_e}{m_e c^2} (t - t_0), \tag{2}$$

x is the dimensionless photon energy given by

$$x(\epsilon) \equiv \frac{\epsilon}{kT_e}, \tag{3}$$

x_0 the dimensionless photon energy at time t_0 and location r_0, and $W_{2,iu}$ are the Whittaker functions. In equation (2) n_e is the electron number density, σ_T the Thomson cross section, c the speeds of light, k the Boltzmann constant, T_e the electron temperature and t the time. In equation (3), ϵ is the photon energy. This solution will make it possible to obtain X-ray spectra without having to solve the Green's function partial differential equation in a numerical way.

For the full derivation of the Green's function solution to the Kompaneets' equation one is advised to consult the paper by Becker [5]. Figure 1 shows the Green's function solution as a function of the dimensionless photon energy x for different values of the dimensionless time y.

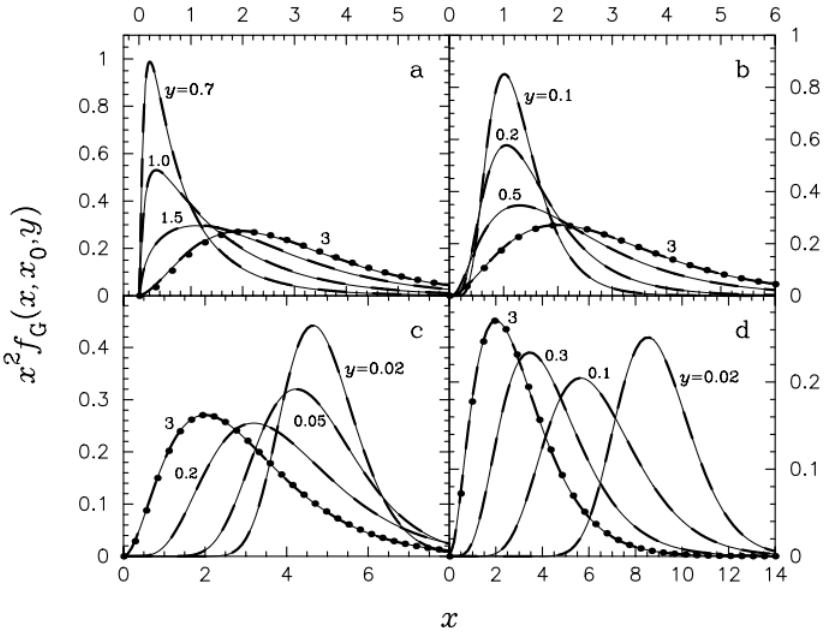

Figure 1: Analytical solution for the Green's function $x^2 f_G(x, x_0, y)$ (eq. (1)) plotted as a function of the dimensionless photon energy x for the indicated values of the dimensionless time y. The initial photon energy is given by (a) $x_0 = 0.1$; (b) $x_0 = 5$; (c) $x_0 = 5$; (d) $x_0 = 10$. The numerical solutions are indicated by the dashed lines and the filled circles show the Wien spectrum. [5]

Figure 1 shows that for each value of x_0 the solution will approach the Wien spectrum for large values of y given by

$$\lim_{y\to\infty} f_G(x, x_0, y) = f_w(x) \equiv \frac{1}{2} e^{-x}. \tag{4}$$

Where the Wien initial spectrum is given by

$$f_0(x) = e^{-x} \tag{5}$$

and by implementing this equation into equation (49) the solution to the Wien initial spectrum will give

$$f(x, y) = e^{-x}. \tag{6}$$

It can be seen that the Wien spectrum is not affected by isothermal Comptonisation. [5]

2.2. Mean photon energy and Inverse-Compton temperature ratio for a mono-energetic initial spectrum

The Green's function obtained in section 2.1 has some properties that can be explored. This can be done with the 'power moments' defined by

$$I_n^G(y) \equiv \int_0^\infty x^n f_G(x, x_0, y) dx. \tag{7}$$

The first property of the Green's function is that it must satisfy the normalisation condition

$$I_2^G(y) = \int_0^\infty x^2 f_G(x, x_0, y) dx = 1 \tag{8}$$

for each value of y. This condition is based on the fact that Compton scattering in the cloud conserves the photon number density. [5]

A second characteristic aspect of the Green's function is the variation of the energy moment given by

$$\bar{x}(y) = I_3^G(y) \equiv \int_0^\infty x^3 f_G(x, x_0, y) dx, \tag{9}$$

and is also called the variation of the mean photon energy. Figure 2 shows the mean photon energy versus the dimensionless time for different values of the initial photon energy x_0.

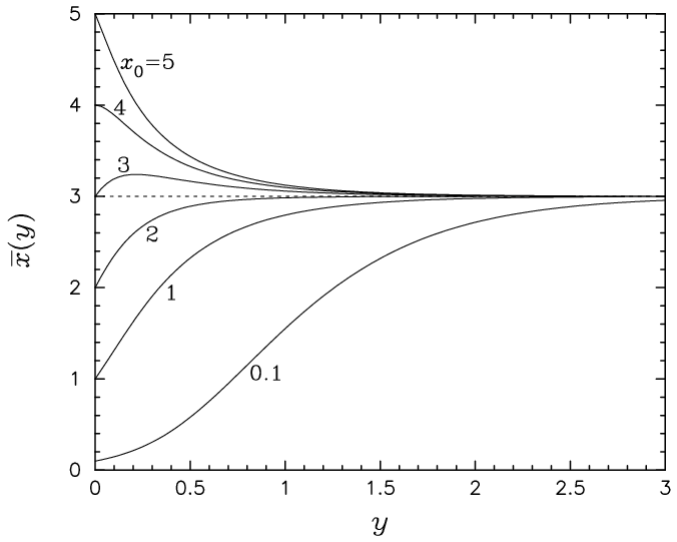

Figure 2: Mean photon energy $\bar{x}$ in case of a mono-energetic initial spectrum, plotted as a function of the dimensionless time y for the indicated values of the initial photon energy x_0.[5]

For each value of x_0 the initial mean photon energy $\bar{x}(0) = x_0$ and for large values of y the mean photon energy will approach a value of 3. The reason for this is that the photon distribution has to approach the Wien's spectrum given by equation (4).

The last property of the Green's function that is examined is the variation of the Inverse-Compton temperature

$$\frac{T_{IC}(y)}{T_e} \equiv \frac{1}{4} \frac{I_4^G(y)}{I_3^G(y)}, \tag{10}$$

where

$$I_4^G(y) \equiv \int_0^\infty x^4 f_G(x, x_0, y) dx, \tag{11}$$

derived from equation (7). Equation (10) provides the closed-form solution which describes the variation of the inverse-Compton temperature for an initially mono-energetic photon distribution. For the derivation to obtain equation (10) one can refer to the paper by Becker [5].
From equation (10) it can be derived that when $T_{IC} < T_e$ the photons gain energy and therefore the mean photon energy $\bar{x}(y)$ increases. When $T_{IC} > T_e$ the photons lose energy and the mean photon energy $\bar{x}(y)$ will decrease. The inverse-Compton temperature for different values of the initial energy x_0 is plotted in Figure 3.

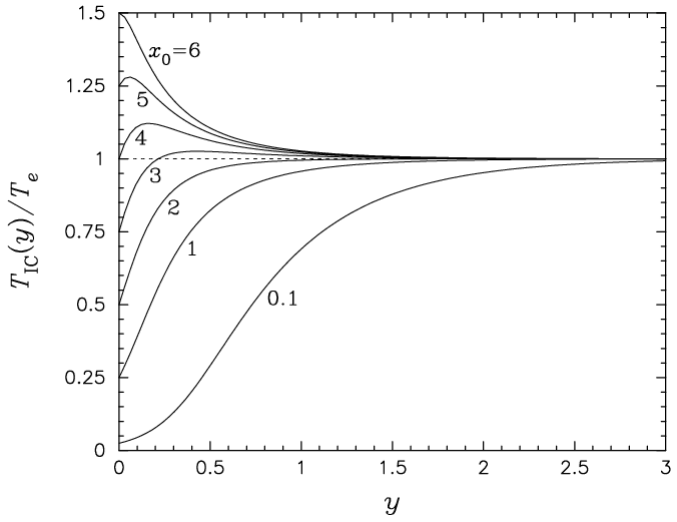

Figure 3: Inverse-Compton temperature ratio T_{IC}/T_e plotted as a function of y in case of a mono-energetic initial spectrum with the indicated value of the initial photon energy x_0.[5]

Figure 3 shows that the inverse-Compton temperature equilibrates to a value of 1 for all values of x_0 in the large y range. This is as expected since $I_3^G \to 3$ and $I_4^G \to 12$, considering that the spectrum should equilibrate to the Wien's spectrum. Since the Wien's spectrum is an eigenfunction of the Kompaneets' equation. [5]

2.3. Time-dependent energy distribution from the Comptonisation of an initial spectrum

The next step is to obtain the particular solution for the time-dependent photon energy distribution that results from a bremsstrahlung or blackbody initial spectrum. Bremsstrahlung radiation is emitted when particles collide. [20] A blackbody initial spectrum is described by equation (37). The initial spectra in units of the constants are then given by

$$f_0(x) = x^{-3}e^{-x}, \tag{12}$$

$$f_0(x) = x^3\left(e^{(x/kT)-1)}\right)^{-1} \tag{13}$$

for a bremsstrahlung initial spectrum [5] and blackbody initial spectrum, respectively. The reason a blackbody initial spectrum is chosen is because it resembles the spectrum of a compact object. [9, 15] Further information about blackbody radiation is provided in Appendix A.1.
In case of a bremsstrahlung initial spectrum, the spectrum initially contains an infinite number of low-energy photons. This makes it impossible to reach the Wien spectrum when $y \to \infty$. Therefore a low-energy cut-off is introduced to recreate the effect of self-absorption. For photons below a specific critical energy, x_*, the mean free path for free-free absorption in the source region gets smaller than the size of the source. Here free-free absorption means that an electron will be free before and after scattering. [5, 1] This critical energy is defined by

$$x_* = 2.6\left(\frac{T_{eff}}{T_e}\right)^2 \ll 1, \tag{14}$$

where T_{eff} is the effective temperature of the radiation. When the photons are below the critical energy the initial bremsstrahlung spectrum reduces to a Planck distribution. The number of photons per unit frequency is proportional to the frequency and therefore a low-energy cut-off arises at the critical energy $x = x_*$. This results in a finite number of photons

in the initial spectrum given by

$$f_0(x) = \begin{cases} 0, & x < x_* \\ x^{-3}e^{-x}, & x \geq x_*. \end{cases} \tag{15}$$

Then the time-dependent photon energy distribution that arises from the Comptonisation of a modified bremsstrahlung initial spectrum is shown in Figure 4.

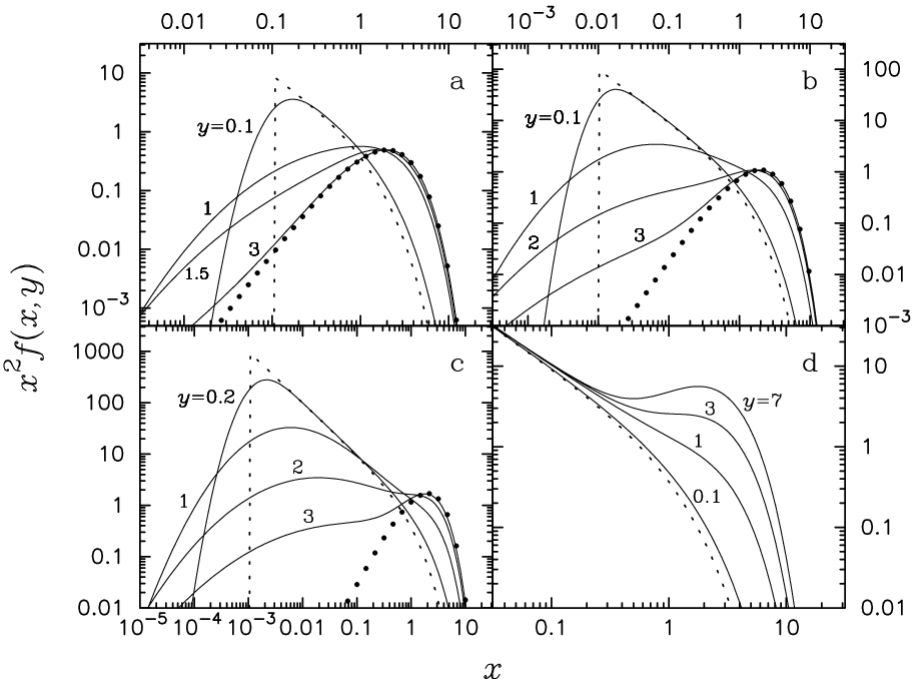

Figure 4: Time-dependent photon energy distribution resulting from the Comptonisation of the modified bremsstrahlung initial spectrum (eq. (49)) as a function of x for the indicated values of the dimensionless time y. The low-energy cut-off values are (a) $x_* = 0.1$; (b) $x_* = 0.01$; (c) $x_* = 0.001$; (d) $x_* = 0$. The dotted lines represent the initial spectra (eq. (12)) and the filled circles represent the equilibrium Wien spectra ($y = \infty$). [5]

Here the spectrum has a low-energy cut-off at $x = x_*$ and a finite number of photons. When $y \to \infty$ the spectrum reduces to the Wien spectrum

$$\lim_{y\to\infty} f(x,y) = \frac{I_2}{2}e^{-x}, \tag{16}$$

where I_2 can be found with equation (8).
As can be seen in Figure 4 the spectrum does not equilibrate to the Wien spectrum when $x_* = 0$, because here the number of photons is infinite. When $x_* > 0$ the number of photons is finite and the Wien equilibrium can be reached. [5]
The case for a blackbody initial spectrum has not been done in the paper by Becker [5] and therefore there is no figure available. However, this will be done as an extension on the paper and is shown in section 3.3.

2.4. Time-dependent escaping photon distribution in case of a spectrum that is initially mono-energetic at time $t = t_0$

Using the Green's function obtained in previous sections, this section obtains the escaping photon distribution for an initially mono-energetic spectrum.

The probability that a photon is still present in the cloud at time $t \geq t_0$ is called the escape time distribution and is given by

$$P(t) = \frac{N_r(t)}{N_0}. \tag{17}$$

Here $N_r(t)$ is the number of photons in the cloud at time t and N_0 the number of photons injected in the cloud at time $t = t_0$. Then the mean escape time of a photon that is still in the cloud at time t is

$$t_{esc}(t) = -\left(\frac{1}{P}\frac{dP}{dt}\right)^{-1}. \tag{18}$$

For a full derivation of the escape time please refer to the paper by Becker [5]. When the escape time is assumed constant the escape time distribution is given by

$$P(t) = e^{-(t-t_0)/t_{esc}}. \tag{19}$$

The number of photons that is in the cloud at time t with energy between x and $x + dx$ is

$$N_x(x,t)dx \equiv P(t)x^2 f(x,y)dx, \tag{20}$$

and the number of photons escaping from the cloud between t and $t + dt$ is then given by

$$\dot{N}_x(x,t)dxdt \equiv t_{esc}^{-1} N_x(x,t)dtdx = t_{esc}^{-1} P(t)dtx^2 f(x,y)dx. \tag{21}$$

Implementing equation (19) in equation (20) will give the number of photons with energy between x and $x + dx$ that escape from the cloud between t and $t + dt$:

$$\dot{N}_x(x,t)dtdx = t_{esc}^{-1} e^{-(t-t_0)/t_{esc}} dtx^2 f(x,y)dx. \tag{22}$$

Here y is the Compton parameter and is defined by equation (2). The time-dependent escaping photon distribution in units of t_{esc} for a spectrum that is initially mono-energetic at time $t = t_0$ is plotted in Figure 5. Here the Compton y-parameter is calculated using the mean value of the Compton y-parameter $\tilde{y}$ with

$$\tilde{y} = t_{esc} n_e \sigma_T c \frac{kT_e}{m_e c^2} = y \frac{t_{esc}}{(t - t_0)}. \tag{23}$$

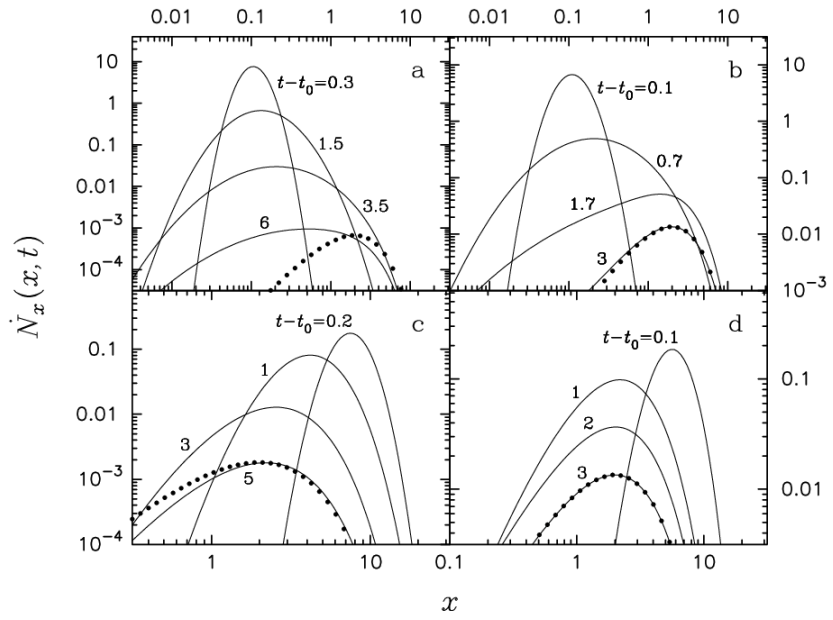

Figure 5: Time-dependent escaping photon energy distribution in units of t_{esc}^{-1} in case of a spectrum that is initially mono-energetic at time $t = t_0$. The elapsed time $t - t_0$ in units of t_{esc} is indicated in each panel. The initial photon energy x_0 and the mean value of the Compton y-parameter $\tilde{y}$ are given by (a) $x_0 = 0.1, \tilde{y} = 0.2$; (b) $x_0 = 0.1, \tilde{y} = 1$; (c) $x_0 = 10, \tilde{y} = 0.2$; and (d) $x_0 = 10, \tilde{y} = 1$. The filled circles represent the Wien spectrum evaluated at time t_{max}, where t_{max} is the maximum time for the sequence of curves in the panel. [5]

The spectrum will eventually reach the Wien's spectrum for large values of $t-t_0$ since most of the radiation has escaped by then. When the initial energy x_0 and/or the mean value of the Compton y-parameter $\tilde{y}$ increases the Wien's spectrum is reached more quickly.

2.5. Time-dependent escaping photon distribution for a continuous injection rate of monochromatic radiation with energy x_0 at $t = 0$

Suppose that the mono-energetic photon source described in section 2.4 is turned on at time $t = 0$ and injects a constant rate of photons. Then the photons that remain in the cloud at time t is given by

$$\begin{aligned} N_x(x,t) &= \int_0^t \dot{N}_0 P(t) x^2 f(x,y) dt_0 \\ &= \int_0^{t/t_{esc}} t_{esc} \dot{N}_0 e^{(t-t_0)/t_{esc}} x^2 f(x, \tilde{y}\,(t-t_0)\,/t_{esc}) dt_0 \end{aligned} \tag{24}$$

Here $\dot{N}_0$ is the rate of injection of fresh photons with dimensionless energy x_0 into the cloud per unit time, $y(t)$ is given by equation (2) and $\tilde{y}$ is given by equation (23).
The radiation that escapes from the cloud is then

$$\dot{N}_x(x,t) = \int_0^{t/t_{esc}} \dot{N}_0 e^{(t-t_0)/t_{esc}} x^2 f(x, \tilde{y}\,(t-t_0)\,/t_{esc}) dt_0. \tag{25}$$

When $t \to \infty$ mono-energetic photon injection, thermal Comptonisation, and photon escape reach a steady-state balance and the escaping photon distribution becomes

$$\dot{N}_x^{std}(x,t) = \frac{\dot{N}_0 x^2}{\tilde{y}} \int_0^\infty e^{-y/\tilde{y}} f(x,y) dy. \tag{26}$$

Figure 6 shows the time-dependent escaping photon energy distribution in units of the injection rate $\dot{N}_0$ versus the energy for mono-energetic photon injection.

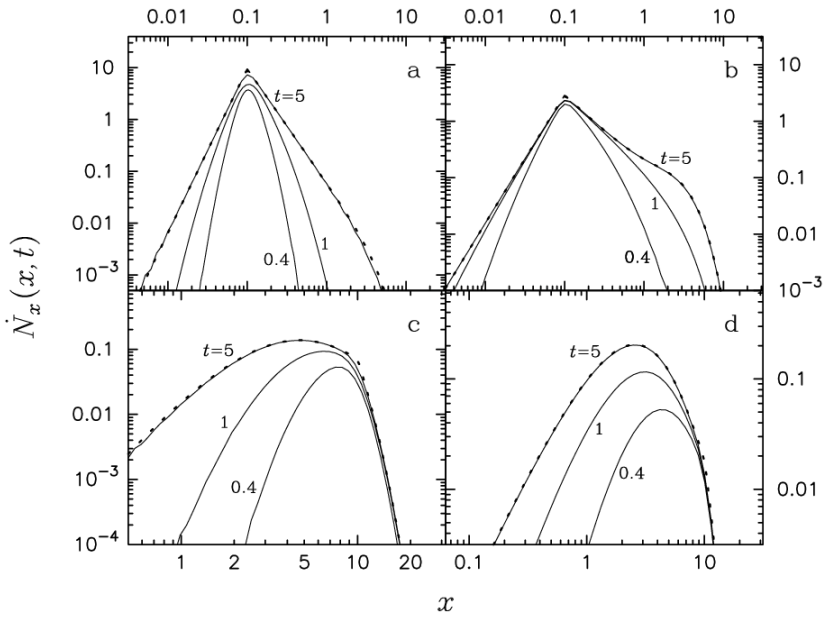

Figure 6: Time-dependent escaping photon energy distribution in units of the injection rate $\dot{N}_0$. Here the injection is continuous with monochromatic radiation with energy x_0, beginning at time $t = 0$. The the time t is indicated in each panel. The values of the initial photon energy x_0 and the mean value of the Compton y-parameter $\tilde{y}$ are given by (a) $x_0 = 0.1, \tilde{y} = 0.2$; (b) $x_0 = 0.1, \tilde{y} = 1$; (c) $x_0 = 10, \tilde{y} = 0.2$ and (d) $x_0 = 10, \tilde{y} = 1$. When time increases the spectrum approaches the steady-state solution (eq. (26)) shown by the filled circles. [5]

Here it is assumed that no photons are initially in the cloud. Whether the steady-state is approached depends on whether the phase of injection is longer then the timescale for the escape of the photons or not.
The spectrum broadens and eventually reaches the steady-state when equilibrium is reached between Comptonisation, photon injection and photon escape. [5]

2.6. Time-dependent escaping photon distribution for a bremsstrahlung and blackbody initial spectrum

The method used in section 2.4 can also be used for a bremsstrahlung and blackbody initial spectra given by equation (12) and (13), respectively. Here $f(x, y)$ in equation (22) is given by equation (49), where f_0 is the bremsstrahlung or blackbody initial spectrum, respectively. Becker [5] has done this for a bremsstrahlung initial spectrum and the result is shown in Figure 7.

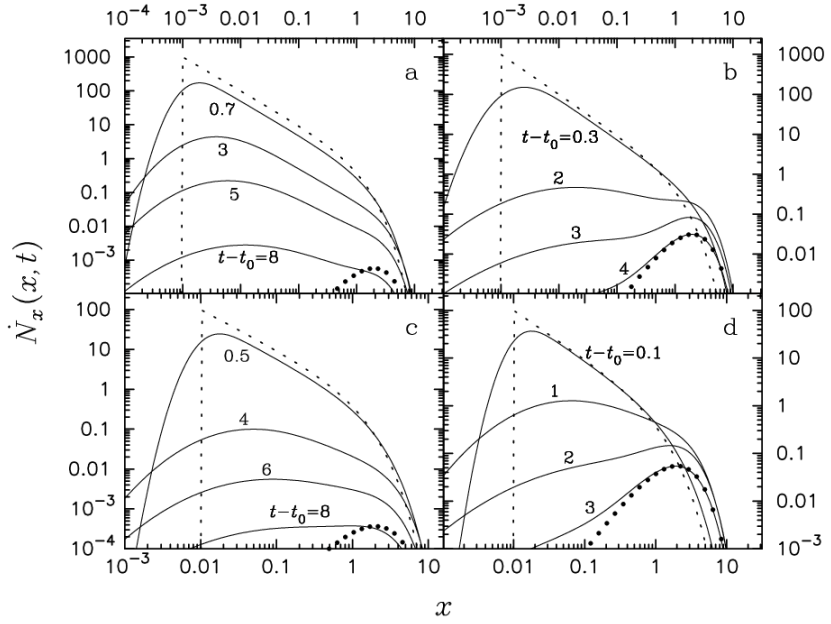

Figure 7: Time-dependent escaping photon energy distribution in units of t_{esc}^{-1} in case of a bremsstrahlung initial spectrum. The elapsed time $t - t_0$ in units of t_{esc} is indicated in each panel. The initial photon energy x_0 and the mean value of the Compton y-parameter $\tilde{y}$ are given by (a) $x_* = 10^{-3}, \tilde{y} = 0.2$; (b) $x_* = 10^{-3}, \tilde{y} = 1$; (c) $x_* = 10^{-2}, \tilde{y} = 0.2$, (d) $x_* = 10^{-2}, \tilde{y} = 1$. The filled circles represent the Wien spectrum evaluated at time t_{max}, where t_{max} is the maximum time for the sequence of curves in the panel. [5]

Figure 7 shows that for small values of the elapsed time $t-t_0$ the escaping photon distribution is similar to the initial spectrum. Here not enough time has elapsed for the photons to escape from the cloud and therefore the spectrum shows that a lot of photons are still escaping. When time increases more and more photons have escaped and the number of photons that escape at this time decreases. When time increases the spectrum starts to approach the Wien spectrum as can be seen in Figure 7. [5] This process can be repeated for a blackbody initial spectrum, which is done in this report (section 3.6).

Finally the same can be done for the escaping photon distribution in units of the injection rate $\dot{N}_0$ as was done in section 2.5. Here $f(x, y)$ is calculated using equation (49), and f_0 is set equal to a bremsstrahlung and a blackbody initial spectrum, respectively.

3. Method and Results

In this section, the model and the results to obtain the escaping photon distribution is described. The Python code for the results presented in sections 3.1 to 3.6 and a separate code for sections 3.7 and 3.8 are available upon request. A full flowchart describing the Python code that recreates the paper by Becker [5] is shown in Figure 29 in Appendix B.1. A flowchart describing the Python code that creates the time-dependent escaping photon distribution for an oscillating temperature or injection rate is shown in Figure 30 in Appendix B.2.
First Figure 2 from Becker[5] is recreated, which is described in section 3.1. Section 3.2 will explain the steps taken to create the mean photon energy and inverse-Compton temperature ratio for a mono-energetic initial spectrum. The solution of the Green's function in section 3.1 is used to find the time-dependent photon energy distribution for a bremsstrahlung and a blackbody initial spectrum in section 3.3. Section 3.4 will describe the steps to plot the time-dependent escaping photon distribution. The plots made for the time-dependent photon distribution in case of the modified bremsstrahlung and a blackbody initial spectrum are described in section 3.5. Section 3.6 will describe the time-dependent escaping photon distribution in units of the injection rate with a continuous injection rate. This is done for monochromatic radiation with energy x_0 and a blackbody initial spectrum.
An oscillation in the initial photon injection $\dot{N}_0$ is applied to study the behaviour of the escaping photon distribution. Here the temperature of the blackbody is kept constant. The blackbody temperature is then set to oscillate while keeping the initial photon injection constant. Oscillating the blackbody will create a more realistic model to compare to the data since in astrophysical applications this temperature is not constant.

3.1. Analytical time-dependent Green's function solution to the Kompaneets' equation

The time-dependent Green's function of the Kompaneets' equation is given by equation (1). To make the code faster it is chosen to program the Whittaker functions given by

$$W_{\kappa,iu}(x) = 2e^{-x/2}x^{1/2}\sum_{n=0}^{\infty}\frac{x_n}{n!}Re\left\{\frac{\Gamma\left(-2iu\right)x^{iu}}{\Gamma\left(-1/2-\kappa-iu\right)}\frac{\left(-1/2-\kappa+iu\right)_n}{\left(1+2iu\right)_n}\right\}, \tag{27}$$

instead of using a built-in function from Python. The Whittaker function in the model will need input parameters. When given the integration values, u, the energy, x, and the value of κ, the function will give back the solution to the Whittaker function.
Furthermore the Green's function in the model will need input values of the energy, x, the initial energy, x_0 and the Compton y-parameter.

To recreate the figure from Becker [5], the values for the input parameters in the model are given by the same values used in the paper by Becker [5]. The solution for the Green's function $x^2 f_G$ plotted using the model is shown in Figure 8. The values used for the parameters y, x and x_0 are indicated in Figure 8.

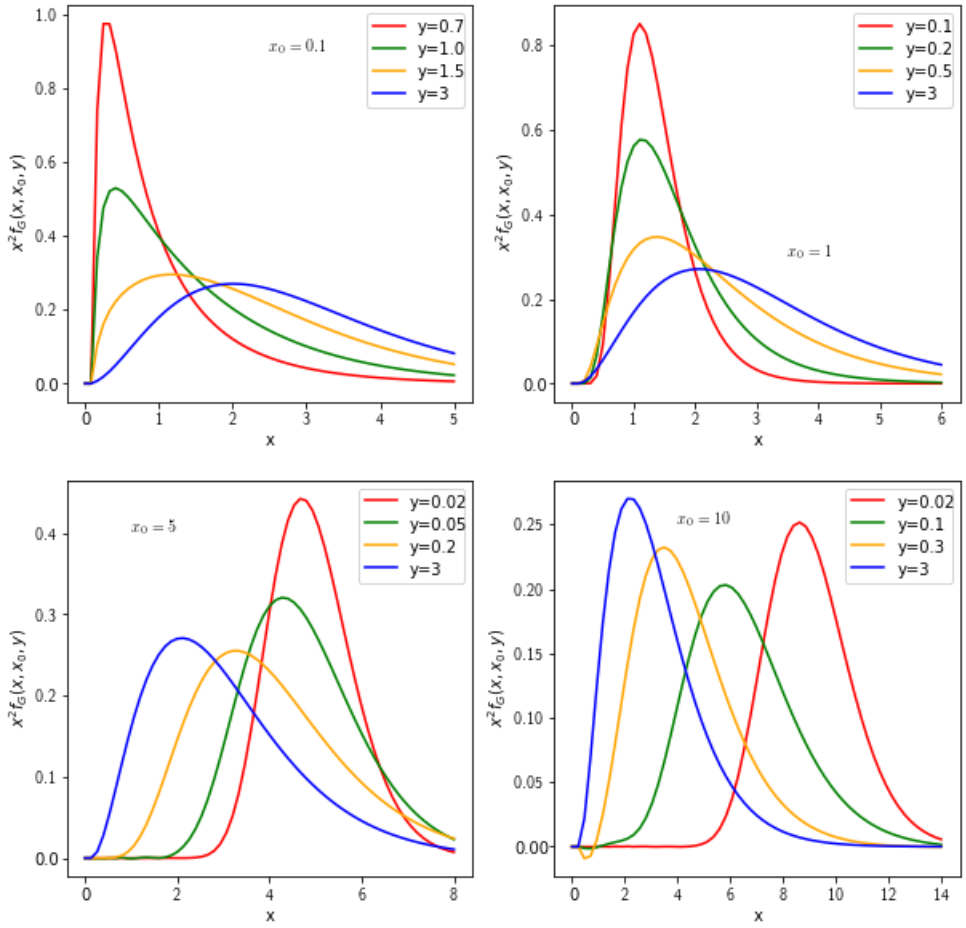

Figure 8: Analytical solution for the Green's function $x^2 f_G(x, x_0, y)$ (eq. (1)) plotted as a function of the dimensionless photon energy x for the indicated values of the dimensionless time y. The initial photon energy x_0 for each panel is indicated in the individual panels.

When comparing Figure 8 to Figure 1 it becomes clear that the figures are identical and therefore it can be assumed that the Green's function in the Python computer model is working and can be used for further calculations.

3.2. Mean photon energy and Inverse-Compton temperature ratio for a mono-energetic initial spectrum

3.2.1. Theoretical model

The Green's function given by equation (1) has some properties that can be explored. One of the properties is that the Green's function must satisfy the normalization condition given by [5]

$$I_2^G(y) = \int_0^\infty x^2 f_G(x, x_0, y) dx = 1. \tag{28}$$

The model contains the function of equation (7) where n is an arbitrary number. Using the Green's function from the model the code can be tested by calculating equation (28) for various values of the initial energy and Compton y-parameter. The result from the model is shown in Table 1 in Appendix C. As shown in the table the values of I_2^G are all around the value of 1. The small deviations from the exact value of 1 are due to round-off errors and numerical errors that arise from the code.

Another interesting property of the Green's function is the variation of the energy moment. This is given by equation (9) and is also called the mean photon energy. Figure 2 represents the mean photon energy as a function of the dimensionless time y from the paper by Becker [5]. Using the Green's function from the model and setting $n = 3$ in equation (7) the mean photon energy obtained from it is shown in Figure 9.

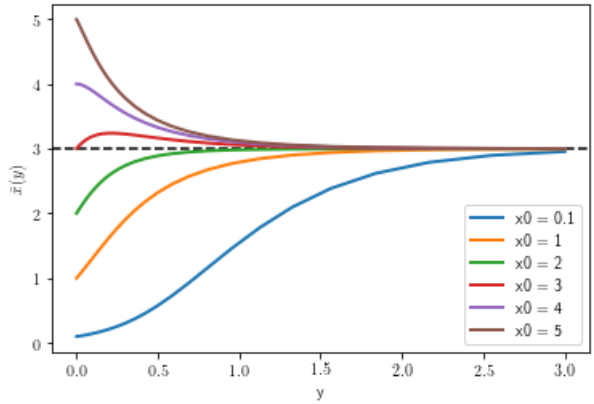

Figure 9: Mean photon energy $\bar{x}$ in case of a mono-energetic initial spectrum, plotted as a function of the dimensionless time y for the indicated values of the initial photon energy x_0.

Here the input parameters in the model for the mean photon energy are n, x_0 and y, and are set to the values from Becker. [5]

Another property of the Green's function is the inverse-Compton temperature of the radiation field given by equation (10) and plotted in Figure 3. The model created in Python takes x_0 and y as input parameters and calculates the inverse-Compton temperature of the radiation field. The result is shown in figure 10.

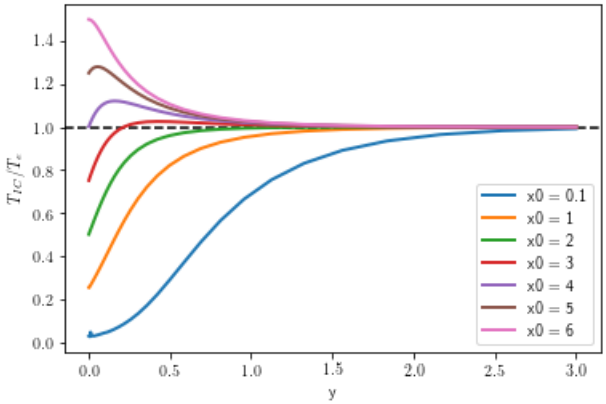

Figure 10: Inverse-Compton temperature ratio T_{IC}/T_e plotted as a function of the dimensionless time y in case of a mono-energetic initial spectrum with the indicated value of the initial photon energy x_0.

3.2.2. Physical explanation

When comparing Figure 9 to Figure 2 it becomes clear that they are the same. It can be seen that the mean photon energy goes to a value of 3. This is expected since the power moments

will approach the Wien spectrum for large values of y. In other words the Green function in equation (7) will be

$$\lim_{y\to\infty} f_G(x,y) = \frac{1}{2}e^{-x}, \tag{29}$$

and thus the mean photon energy is

$$\lim_{y\to\infty} I_3 = \int_0^\infty x^3 \frac{1}{2}e^{-x}dx = 3. \tag{30}$$

Figure 10 is the same as Figure 3 and thus it can be said that the Python model works properly. It can be seen that T_{IC}/T_e goes to 1 as time goes to infinity. This is consistent with the expectation since $I_3 \to 3$ and $I_4 \to 12$ and thus equilibrate to the Wien form.
Another aspect that can be seen from Figure 10 is that for $x_0 < 4$ the photons are initially cooler than the electrons. This causes the initial increase in the mean photon energy from Figure 9. When $x_0 > 4$ the mean photon energy decreases due to the fact that energy is initially transferred from the photons to the electrons. When $x_0 = 3$ the mean energy of the photons start to increase since their energy is lower than the temperature of the electrons. At $y \sim 0.25$ the mean photon energy reaches a maximum and starts decreasing since from this point the inverse-Compton temperature exceeds the electron temperature and therefore the photons start losing energy. [5]

3.3. Time-dependent energy distribution from the Comptonisation of an initial spectrum

3.3.1. Theoretical model

The time-dependent Comptonisation of an optically thin bremsstrahlung initial spectrum with a low-energy cut-off at $x = x_*$ and a finite number of photons can be calculated using the Green's function. The solution to a function $f(x,y)$ corresponding to an arbitrary initial spectrum $f_0(x)$ can be found using equation (49). In case of an optically thin bremsstrahlung initial spectrum the initial spectrum $f_0(x)$ is defined by equation (12) and the Green's function is defined by equation (1). The Python-model takes the Compton y-parameter, the energy x, and the critical energy x_* as input parameters and calculates the Comptonised bremsstrahlung spectrum for a bremsstrahlung initial spectrum.

Figure 11 shows the result for a bremsstrahlung initial spectrum with low-energy cut-off at $x = x_*$ and a finite number of photons. The input parameter values used in the model are also shown in the figure.

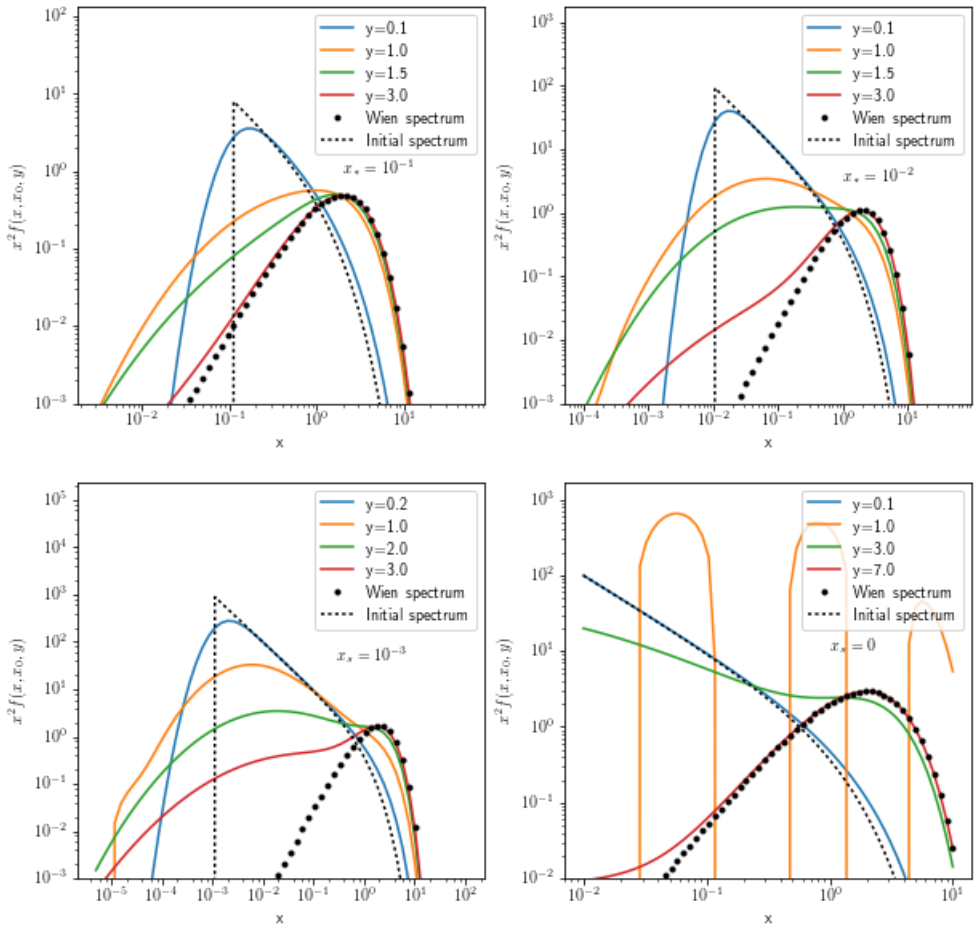

Figure 11: Time-dependent photon energy distribution resulting from the Comptonisation of the modified bremsstrahlung initial spectrum (eq. (49)) as a function of x for the indicated values of the dimensionless time y. The dotted lines represent the initial spectra (eq. (12)) and the filled circles represent the equilibrium Wien spectra ($y = \infty$).

The same time-dependent Comptonisation can be done for a blackbody initial spectrum with temperature kT given by equation (13). In the model, the input parameters for the calculation of the time-dependent Comptonisation of a blackbody initial spectrum are the Compton y-parameter, the energy x and the temperature of the blackbody, kT. Here the temperature kT is given in units of the electron temperature kT_e and is a fraction of the coronal temperature. The result is shown in Figure 12 and the values of the input parameters are also indicated in the figure.

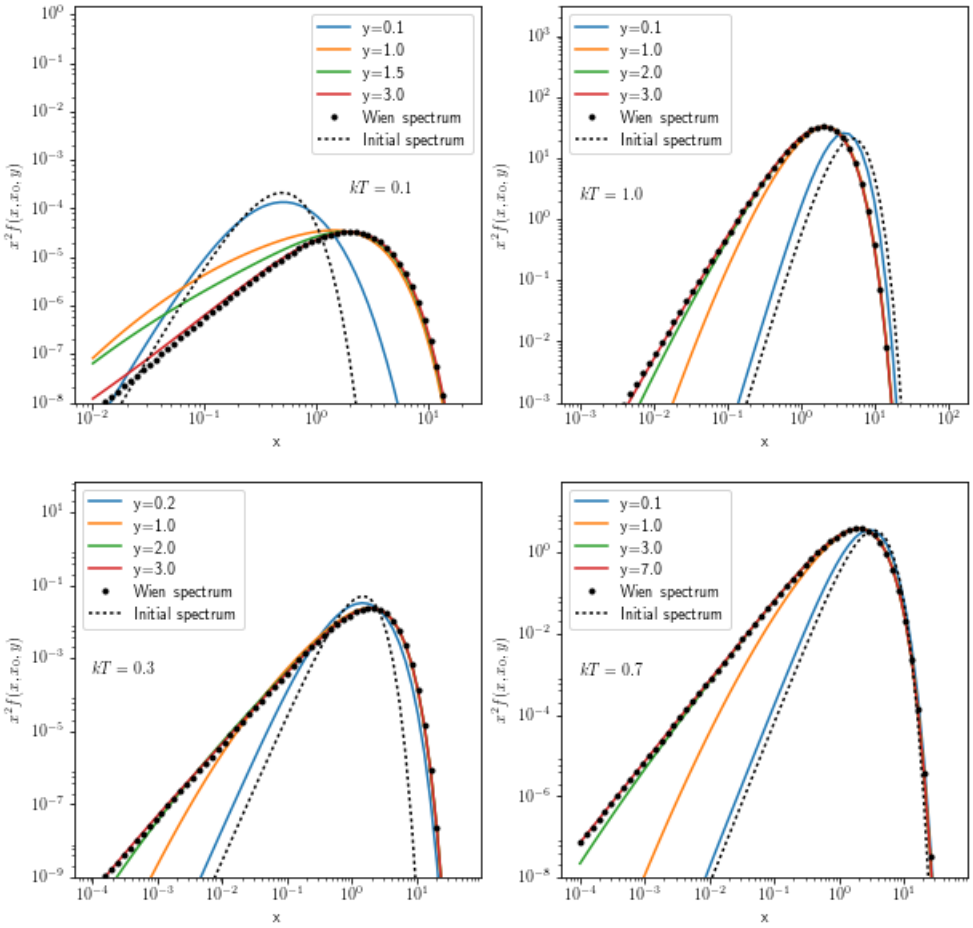

Figure 12: Time-dependent photon energy distribution resulting from the Comptonisation of the blackbody initial spectrum (eq. (49)) as a function of x for the indicated values of the dimensionless time y. The dotted lines represent the initial spectra (eq. (49)) and the filled circles represent the equilibrium Wien spectra ($y = \infty$).

3.3.2. Physical explanation

It can be seen that when the Compton y-parameter approaches large values the spectrum equilibrates to a Wien's spectrum given by equation (4). The reason it equilibrates to this Wien's function is because it is an eigenfunction of the Kompaneets' equation. The dotted lines in Figure 11 represent the initial bremsstrahlung spectrum given by equation (12). For small values of the Compton y-parameter, and thus at small values of the dimensionless time, the time-dependent photon energy distribution is similar to the initial spectrum. It will deviate from the initial spectrum and equilibrate to a Wien spectrum when the time increases. When x_* increases the spectrum equilibrates to a Wien spectrum more rapidly.

The spectrum for $y = 3$ in the panel where $x_* = 0$ in Figure 11 has numerical round-off errors due to the fact that $x_* = 0$ here is set to $x_* = 10^{-5}$ to represent a value close to zero and therefore has a wiggle. The equation that is used to calculate the time-dependent photon energy distribution is different than the one used in the paper by Becker [5]. Therefore the other values of y in the bottom right panel of Figure 11 compared to Figure 4 are different. It can be seen in Figure 12 that at low values of the Compton y-parameter and thus at small values of the dimensionless time the spectrum resembles the initial blackbody spectrum. When time increases the spectrum will equilibrate to a Wien spectrum given by setting $y = \infty$

in equation (13). When the value of the temperature increases the time-dependent photon energy distribution will equilibrate to a Wien spectrum more rapidly. Because in this case, the blackbody has a temperature that is closer to that of the corona and therefore they reach equilibrium faster.

3.4. Time-dependent escaping photon distribution in case of a spectrum that is initially mono-energetic at time $t = t_0$

3.4.1. Theoretical model

The number of photons with energy between x and $x + dx$ escaping from the cloud in the time interval between t and $t + dt$ is given by equation (22). For an initially mono-energetic spectrum, $f(x, y)$ is set to the Green's function given by equation (1). Calculating the escaping photon distribution with the model can be done by giving the values for the input parameters of the mean value of the Compton y-parameter $\tilde{y}$, the energy x, the elapsed time $t - t_0$ and the initial energy x_0. Here $\tilde{y}$ is used in the model to calculate the dimensionless time y by using equation (23). The time-dependent escaping photon distribution for a spectrum that is initially mono-energetic is shown in Figure 13. Here the values for the input parameters used for the model are shown in the figure.

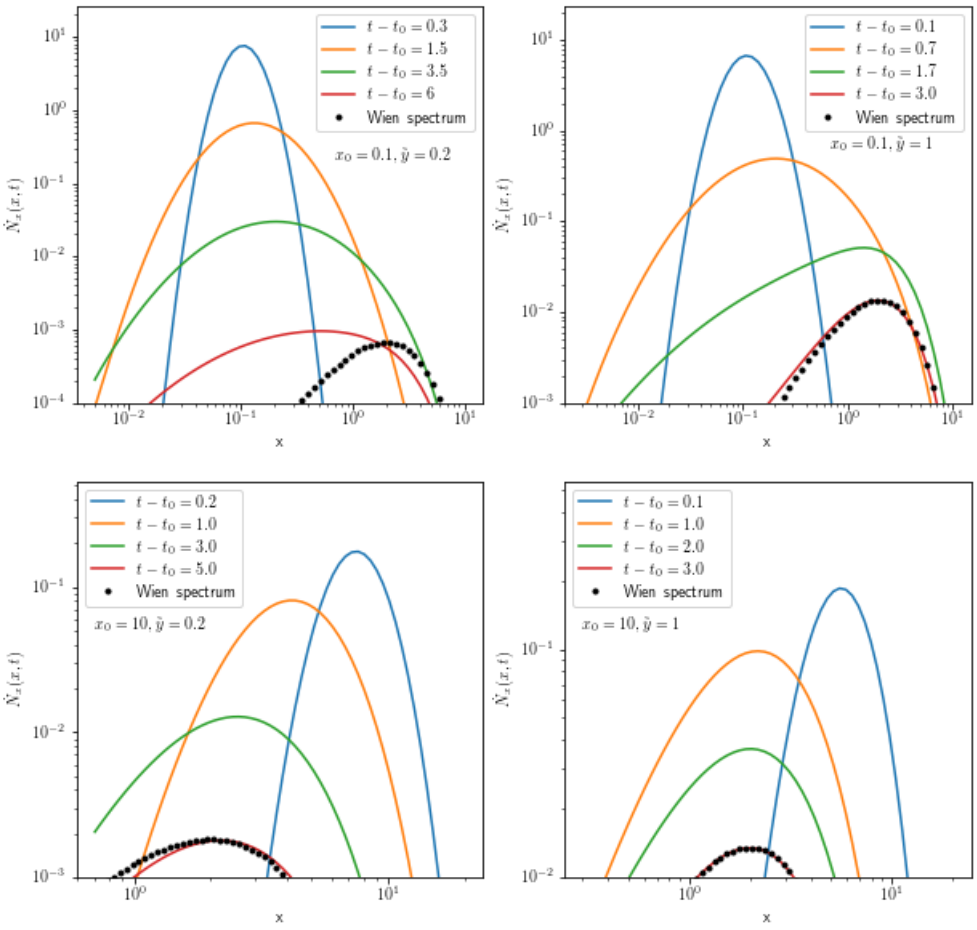

Figure 13: Time-dependent escaping photon energy distribution in units of t_{esc}^{-1} in case of a spectrum that is initially mono-energetic at time $t = t_0$. The elapsed time $t - t_0$ in units of t_{esc}, the initial photon energy x_0 and the mean value of the Compton y-parameter $\tilde{y}$ are indicated in each panel. The filled circles represent the Wien spectrum evaluated at time t_{max}, where t_{max} is the maximum time for the sequence of curves in the panel.

3.4.2. Physical explanation

The spectra shown in Figure 13 can be interpreted as the spectra that one observes outside the corona when the initial burst of monochromatic radiation is changed by electron scattering. When the elapsed time $t - t_0$ is small, not much scattering has occurred and therefore the spectrum of the escaping photon distribution is narrow and centred on the initial energy x_0. When $t - t_0$ increases more photons escape the corona and this will eventually lead to the spectrum resembling the Wien spectrum. As expected the equilibration to the Wien spectrum occurs more rapidly when x_0 increases and/or when $\tilde{y}$ increases. The higher the energy of the monochromatic input spectrum, the quicker the photons reach equilibrium in the corona. When $y >> 1$ the total photon energy in the spectrum is significantly altered (Comptonisation occurs faster). When $y << 1$ the spectrum takes longer to Comptonise and reach the Wien spectrum. [5]

3.5. Time-dependent escaping photon distribution for a continuous injection rate of monochromatic radiation with energy x_0 at $t = 0$

3.5.1. Theoretical model

The time-dependent escaping photon energy distribution in units of the injection rate $\dot{N}_0$ is given by equation (25). When $f(x, \tilde{y}\epsilon)$ is equal to the Green's function, the time-dependent escaping photon distribution corresponds to the continuous injection of monochromatic radiation with energy x_0, which begins at $t = 0$. The Python-model to calculate this takes the mean value of the Compton y-parameter, $\tilde{y}$, given by equation (23), the energy, x, the elapsed time, t, and the initial energy, x_0, as input parameters. The spectra obtained are shown in Figure 14. The values used for the input parameters of the model are indicated in the figure.

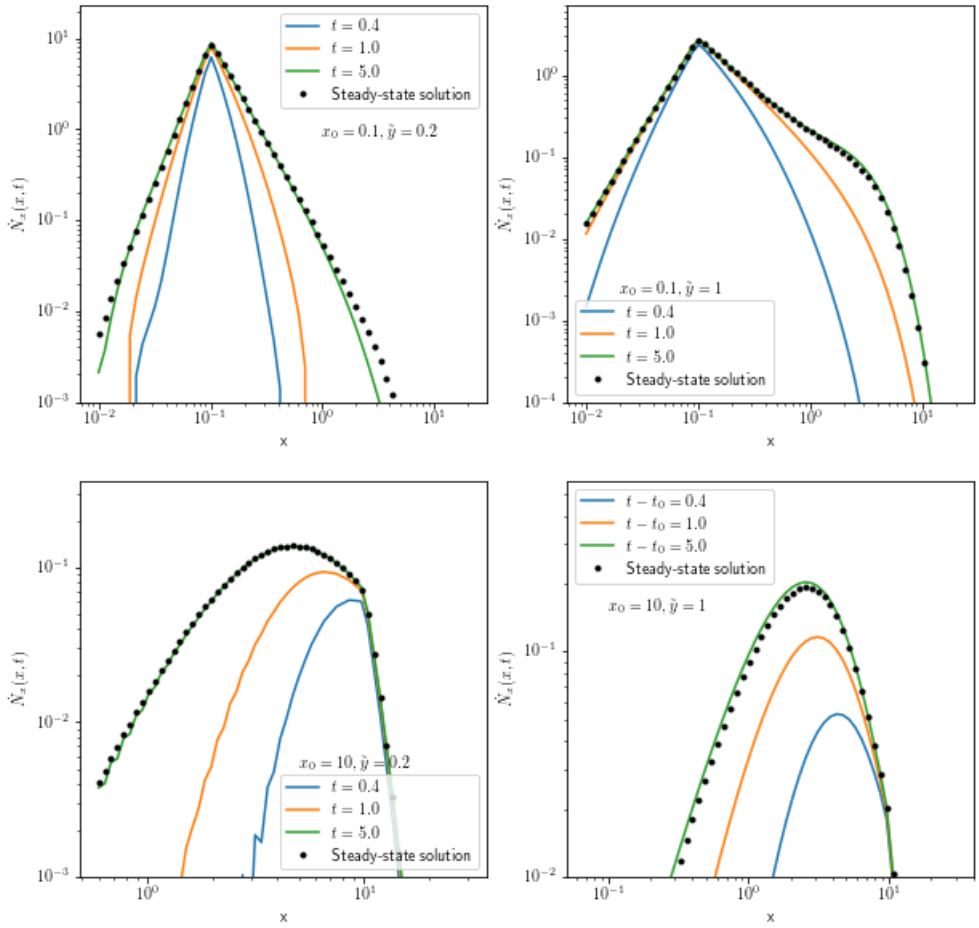

Figure 14: Time-dependent escaping photon energy distribution in units of the injection rate $\dot{N}_0$. Here the injection is continuous with monochromatic radiation with energy x_0, beginning at time $t = 0$. The initial photon energy, x_0, the time, t, and the mean value of the Compton y-parameter, $\tilde{y}$, are indicated in each panel. The filled circles indicate the steady-state spectrum.

3.5.2. Physical explanation

Figure 14 shows that when time increases the spectrum broadens and starts to resemble the steady-state solution given by equation (26). This is expected since a balance is obtained between mono-energetic photon injection, thermal Comptonisation and photon escape.

3.6. Time-dependent escaping photon distribution for a bremsstrahlung and blackbody initial spectrum

3.6.1. Theoretical model

The results obtained in section 3.4 and 3.5 are for a mono-energetic initial spectrum, but can also be obtained for different initial spectra. In this section, the time-dependent escaping photon energy distribution is obtained for a bremsstrahlung initial spectrum and a blackbody initial spectrum. In other words, the function $f(x, \tilde{y}\epsilon)$ given by equation (49) and f_0 in this equation is given by the bremsstrahlung initial spectrum (equation (12)) and blackbody initial spectrum (equation (13)).

The model for the time-dependent escaping photon energy distribution in units of t_{esc} takes

the mean value of the Compton y-parameter, $\tilde{y}$, the energy, x, the elapsed time, $t - t_0$, and the low-energy cut-off, x_*, as input parameters when the initial spectrum is a bremsstrahlung spectrum. When the initial spectrum is a blackbody spectrum the input parameters for the model are the mean value of the Compton y-parameter, $\tilde{y}$, the energy, x, the elapsed time, $t - t_0$, and the temperature of the blackbody, kT, in units of the electron temperature T_e.

Figure 15 and Figure 16 show the time-dependent escaping photon energy distribution in units of t_{esc} for the bremsstrahlung initial spectrum and blackbody initial spectrum respectively.

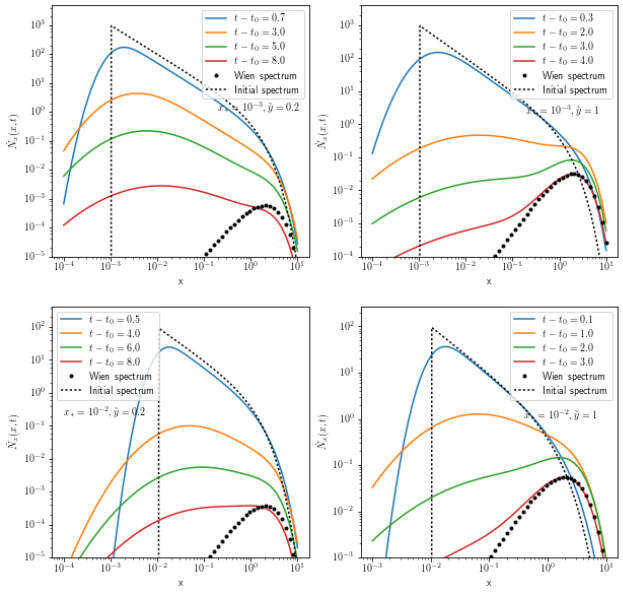

Figure 15: Time-dependent escaping photon energy distribution in units of t_{esc}^{-1} in case of a bremsstrahlung initial spectrum. The elapsed time, $t - t_0$, in units of t_{esc}, the initial photon energy, x_0, and the mean value of the Compton y-parameter, $\tilde{y}$, are indicated in each panel. The filled circles represent the Wien's spectrum evaluated at time t_{max}, where t_{max} is the maximum time for the sequence of curves in the panel.

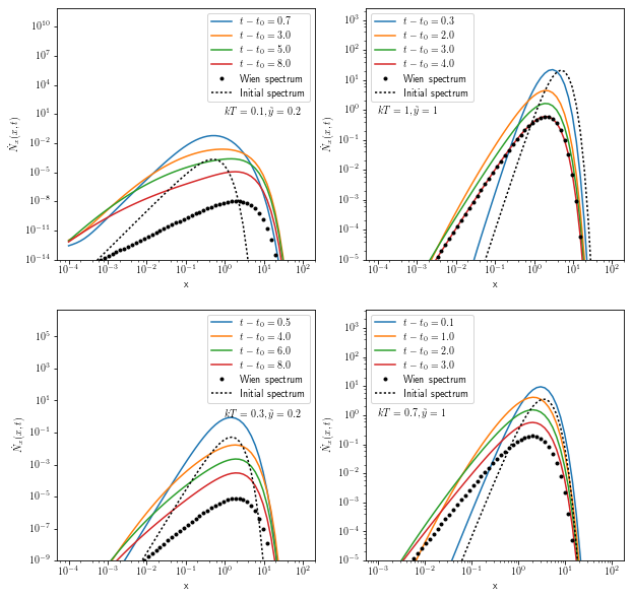

Figure 16: Time-dependent escaping photon energy distribution in units of t_{esc}^{-1} in case of blackbody spectrum. The elapsed time, $t - t_0$, in units of t_{esc}, the corona temperature in units of the electron temperature, kT, and the mean value of the Compton y-parameter, $\tilde{y}$, are indicated in each panel. The filled circles represent the Wien spectrum evaluated at time t_{max}, where t_{max} is the maximum time for the sequence of curves in the panel.

To calculate the time-dependent escaping photon energy distribution in units of the injection rate $\dot{N}_0$ for a blackbody initial spectrum the model takes the mean value of the Compton y-parameter, $\tilde{y}$, the energy, x, the time, t, and the temperature, kT, in units of the electron temperature, kT_e, as input parameters. The result is shown in Figure 17.

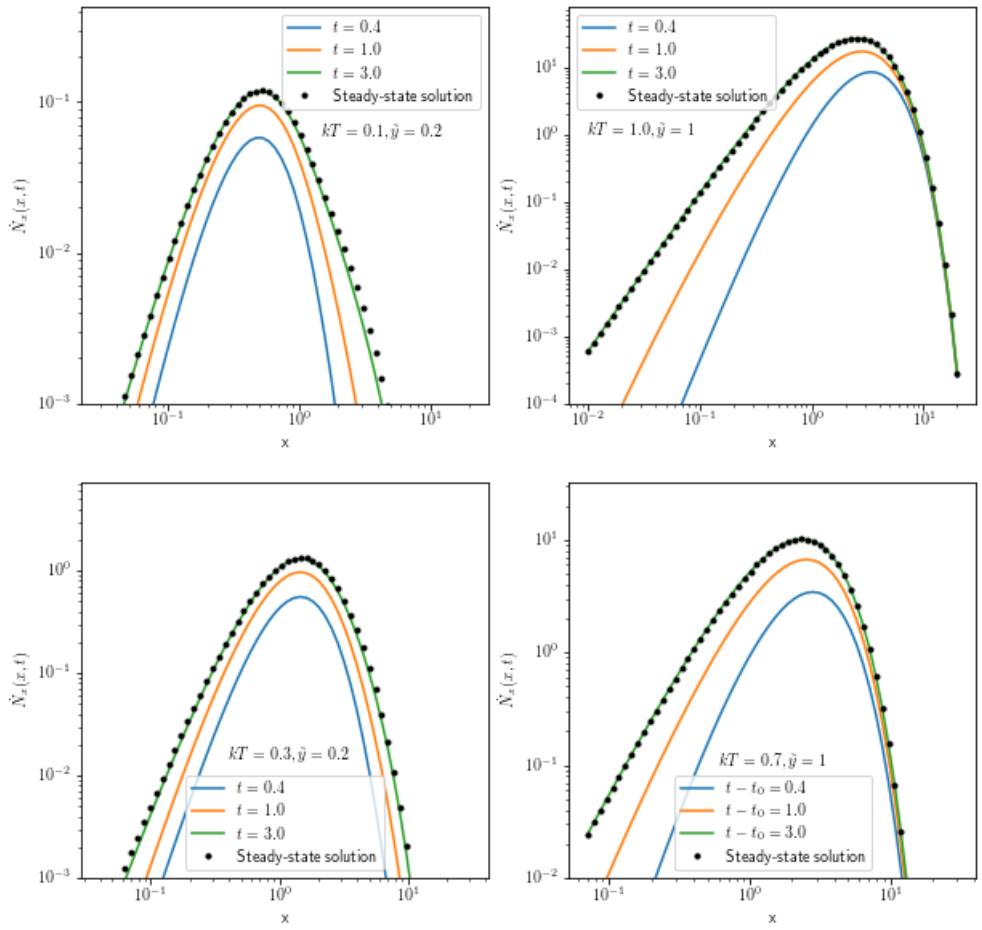

Figure 17: Time-dependent escaping photon energy distribution in units of the injection rate $\dot{N}_0$ for a blackbody initial spectrum. The corona temperature in units of the electron temperature kT, the time t and the mean value of the Compton y-parameter, $\tilde{y}$, are indicated in each panel. The filled circles represent the steady-state spectrum.

3.6.2. Physical explanation

Figure 15 can be compared to Figure 7 and it is seen that they are similar. Figure 15 and Figure 16 also show that for small values of $t - t_0$ the escaping spectrum approaches the initial spectrum. When the time increases the spectrum hardens and the Wien spectrum is approached.
In the low energy part of the spectrum, the spectrum increases with decreasing low-energy cut-off, x_*, in the case of the bremsstrahlung initial spectrum, because when the low-energy cut-off is lower it takes longer to up-scatter the soft photons. The amplitude of the spectrum at energies around the Wien peak also increases when the mean value of the Compton y-parameter increases. This is due to the fact that there is competition between the Comptonisation and photon escape. It can also be seen that when x_* or $\tilde{y}$ increase, the spectrum equilibrates to the Wien spectrum more rapidly. [5]
The fact that the spectrum equilibrates to the Wien spectrum more rapidly when $\tilde{y}$ increases also applies to the blackbody spectrum. Here the spectrum reaches the Wien spectrum more rapidly when the temperature of the blackbody increases.

The next step is to calculate the time-dependent escaping photon energy distribution in units of the injection rate $\dot{N}_0$ for a blackbody initial spectrum. In this case, the spectrum is only

calculated for a blackbody spectrum and not a bremsstrahlung initial spectrum, since a compact object resembles a blackbody initial spectrum and not a bremsstrahlung initial spectrum.[9, 15] The reason it was done for a bremsstrahlung initial spectrum in the previous sections is to verify the Python-model.
It can be seen in Figure 17 that when the temperature of the blackbody, kT, or the value of the mean value of the Compton y-parameter, $\tilde{y}$, increases, the spectrum reaches the Wien spectrum more rapidly. When the Compton y-parameter increases the total photon energy in the spectrum is significantly altered and Comptonisation occurs more rapidly and thus equilibrium is reached faster.[5] When the temperature of the blackbody is higher, it will be closer to the temperature of the corona and they will reach equilibrium more quickly.

3.7. Time-dependent escaping photon distribution for a bremsstrahlung and blackbody initial spectrum with a varying injection rate $\dot{N}_0$

3.7.1. Theoretical model

The solutions obtained in the previous sections are for a transient and/or steady-state, but now it is possible to add a perturbation. In the previous sections, it was assumed that the injection of photons into the corona is continuous, which will lead to a balance between the mono-energetic photon injection, thermal Comptonisation and photon escape. The most ideal model will represent the reality and since the Python-model in the previous sections is not a very realistic model partly due to the continuous photon injection, some extra aspects can be added. One aspect is to vary the photon injection from the source. Since any oscillation or periodic signal can be represented by a Fourier series, thus a summation of sine functions, the oscillation of the injection of photons into the corona will be described by a sine function. By using this form of oscillation it will also be easier to add more complicated functions. For the model, the time-dependent escaping photon distribution with an oscillating photon injection rate is given by

$$\dot{N}_x\left(x,t\right)=\int_0^{t/t_{esc}}\dot{N}_0\left(1+A\sin\left(wt_0\right)\right)e^{-\frac{t-t_0}{t_{esc}}}x^2 f\left(x,x_0,\tilde{y}\left(\frac{t-t_0}{t_{esc}}\right)\right)dt_0. \tag{31}$$

Using equation (31) it is possible to obtain the light curves for specific energies and study the behaviour for different values of the angular frequency and amplitude. In this case the function $f(x,x_0,y)$ will be defined by equation (49) where f_0 is a blackbody initial spectrum (equation (13)).

By examining the section of the light curve where it has reached equilibrium for different energies, angular frequencies and temperatures, the response of the light curve can be studied. Here the amplitude is kept at a value of 0.9 and the temperature is set to be $kT = 1.0$ and $kT = 0.1$. Here $kT = 1.0$ means that the temperature of the blackbody is equal to the temperature of the corona and $kT = 0.1$ means that the blackbody temperature is 10 percent of that of the corona and thus the corona is 10 times hotter. If the photon has more energy, it gives energy to the electron. Therefore, a corona with a lower or equal temperature than that of the blackbody will cause down-scattering. If the photon has less energy, it gains energy from the electron. Thus a corona that has a higher temperature than the blackbody, and thus higher energy levels, will cause up-scattering. (See Appendix A.3 for more information about Comptonisation)
Finally, the value of the angular frequency is set to $\omega = 2\pi$ and $\omega = 2\pi\sqrt{3}$. Figure 18 shows the light curves.

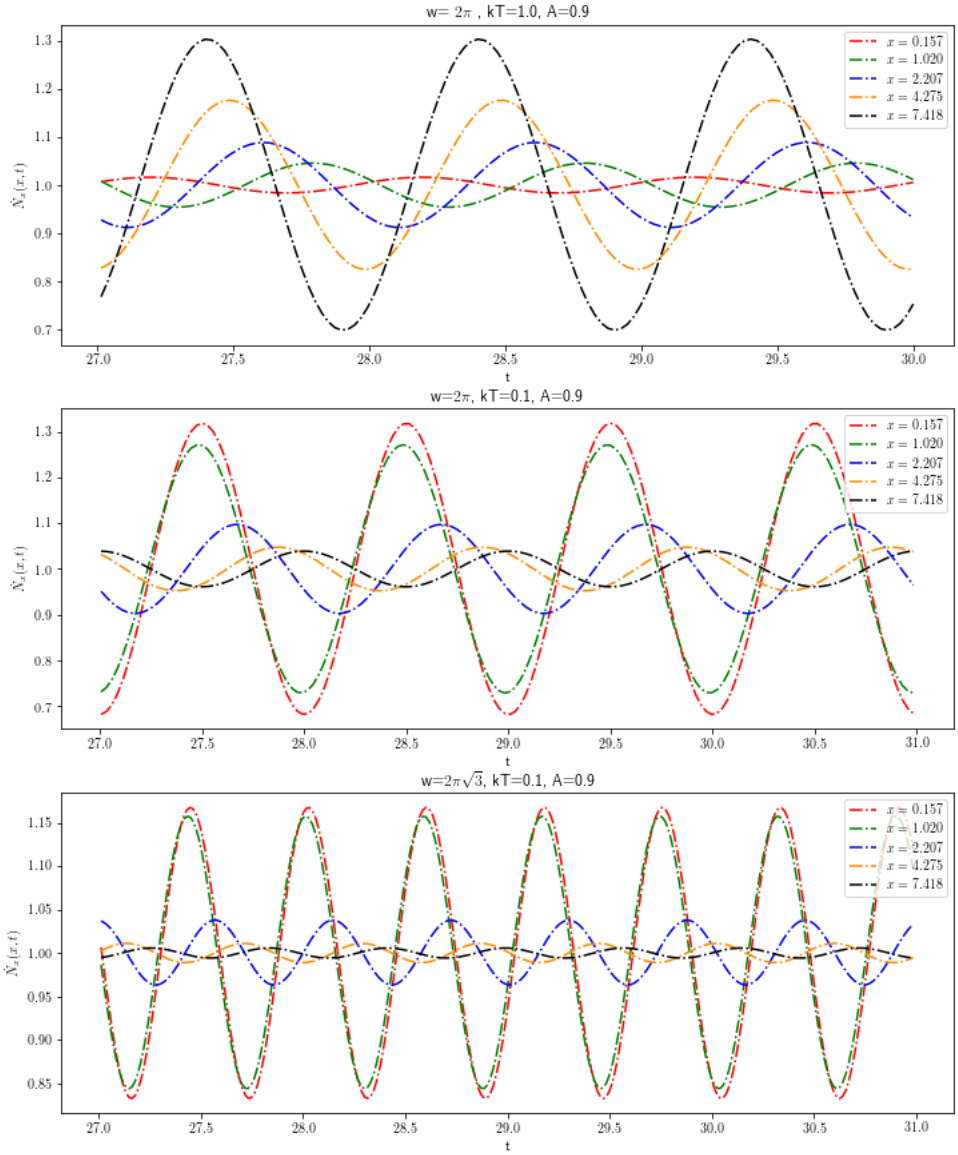

Figure 18: Time-dependent escaping photon energy distribution in units of the injection rate $\dot{N}_0$ for a blackbody initial spectrum with a varying injection rate. In the top panel $kT = 1.0$, $\tilde{y} = 1.0$, $A = 0.9$ and $\omega = 2\pi$. In the middle panel $kT = 0.1$, $\tilde{y} = 1.0$, $A = 0.9$ and $\omega = 2\pi$. In the bottom panel $kT = 0.1$, $\tilde{y} = 1.0$, $A = 0.9$ and $\omega = 2\pi\sqrt{3}$. The light curve is selected in the large time range to obtain only the part that has reached equilibrium.

Not only the light curve can produce some useful information, but so can the spectra. A spectrum refers to the time-dependent escaping photon distribution versus the energy at different values of the time t. A model is created that shows the change of the spectra over time and is available upon request. Figure 34 shows the spectrum with a slider over the time where it is set on $t = 16.31[t_{esc}^{-1}]$.

Finally, an interesting aspect to study is the Fast Fourier Transform (FFT) of the light curves. This will result in a power spectrum with a Lorentzian form and is shown in Figure 19 for a temperature of $kT = 0.1$, amplitude of $A = 0.9$ and different angular frequencies of $\omega = \frac{2\pi}{\sqrt{3}}$, $\omega = 2\pi$ and $\omega = 2\pi\sqrt{3}$.

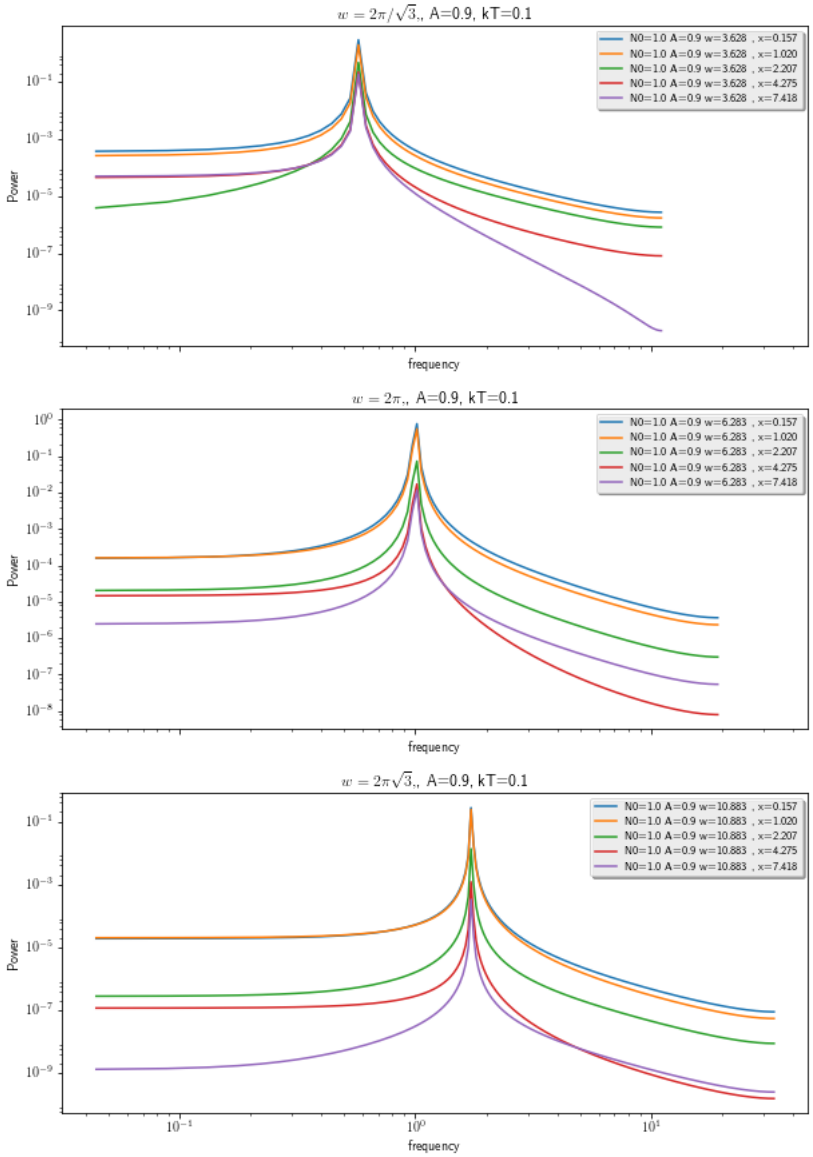

Figure 19: FFT power spectra of the time-dependent escaping photon energy distribution light curves in units of the injection rate $\dot{N}_0$ for a blackbody initial spectrum with a varying injection rate. In the top panel $kT = 0.1$, $\tilde{y} = 1.0$, $A = 0.1$ and $\omega = \frac{2\pi}{\sqrt{3}}$. In the middle panel $kT = 0.1$, $\tilde{y} = 1.0$, $A = 0.1$ and $\omega = 2\pi$. In the bottom panel $kT = 0.1$, $\tilde{y} = 1.0$, $A = 0.1$ and $\omega = 2\pi\sqrt{3}$. The light curve is selected in the large time range to obtain only the part that has reached equilibrium.

3.7.2. Physical explanation

Figure 31, Figure 32 and Figure 33 in Appendix D show; the oscillation, the time-dependent escaping photon distribution with continuous injection rate, and the time-dependent escaping photon distribution with varying injection rate. This is plotted in a three-panel graph for different combinations of the angular frequency and amplitude. It becomes clear that with increasing angular frequency the oscillatory part becomes less prominent in the light curve. Figure 32 shows the light curve for continuous photon injection with the oscillatory part, which indicates that when the angular frequency increases the light curves take more time to reach the equilibrium state. When increasing the amplitude of the oscillation it will result in a more rapid reach of the equilibrium state. The light curves for the time-dependent escaping

photon distribution with varying injection rate that are shown in Figure 31, Figure 32 and Figure 33 are not simply the time-dependent escaping photon distribution with continuous injection rate with a sine function on top of it. Here the light curves are modified by Comptonisation.

The top panel in Figure 18 clearly shows that with decreasing energy the light curves shift to the right and get a phase lag with respect to the lower energy light curve. These phase lags are caused by the down-scattering mentioned before. In Figure 35 in Appendix F the phase lags for each value of the angular frequency is plotted versus the energy at the QPO frequency.
The amplitude decreases with decreasing energy, unlike the second panel where the amplitude increases with decreasing energy. It is tested if this is caused by Comptonisation by running the model and determining the time-dependent escaping photon distribution only for a blackbody with varying injection rate without the Green's function. When plotting the light curves they are all the same for each energy and therefore it is now known that the decrease or increase in amplitude with energy is caused by Comptonisation.
The phase lags for the second panel increases with increasing energy completely reversing the effect seen in the top panel. This can be explained by the fact that since the corona is now hotter than the blackbody the up-scattering causes these phase lags.
When comparing the panel on the bottom with the middle panel, only the angular frequency has changed. This plot shows that there is a strong effect on the amplitude when the angular frequency changes, but the phase lags stay the same. This indicates that the phase lags are only dependent on temperature changes and not on changes in the angular frequency, which was expected since the up- and down-scattering is dependent on temperature. This plot also shows that the amplitude is dependent on temperature as well as energy and angular frequency.

When changing the time, the spectra will move up and down with a wiggle as a result of the oscillation. This effect is best shown by using a slider for the time or making an animation over the time which can clearly show the changes in the spectra.

Finally, Figure 19 shows that the peak of the power spectrum shifts to the right with increasing angular frequency as expected since the frequency is defined by

$$f = \frac{\omega}{2\pi} \tag{32}$$

and thus the peak of the power spectrum will be at a higher frequency value when the angular frequency increases. These peaks are similar to the QPOs observed in the power spectra of X-ray binaries and therefore the model can be used to compare with the data. Here there is only one fundamental harmonic since the injection is sinusoidal. The power spectrum is broadened compared to a power spectrum of a perfect sine (which is a delta function). This broadening is due to the escape time of the photons and Comptonisation that occurs in the corona.

3.8. Time-dependent escaping photon distribution for a blackbody initial spectrum with a varying temperature

3.8.1. Theoretical model

In the previous section a perturbation in the photon injection rate was added to the model. Now instead of varying the photon injection rate, it is possible to vary the temperature of the blackbody and study the behaviour of the time-dependent escaping photon distribution while the photon injection rate is kept constant. The temperature will vary with a sine function again, the reason for this was discussed in the previous section. This leads to the time-dependent

escaping photon distribution given by

$$\dot{N}_x\left(x,t\right)=\int_0^{t/t_{esc}}\dot{N}_0e^{-\frac{t-t_0}{t_{esc}}}x^2f\left(x,x_0,\tilde{y}\left(\frac{t-t_0}{t_{esc}}\right),\left(1+A\sin\left(wt_0\right)\right)kT\right)dt_0. \tag{33}$$

Where $f\left(x,x_0,\tilde{y}\left(\frac{t-t_0}{t_{esc}}\right),\left(1+A\sin\left(wt_0\right)\right)kT\right)$ is given by equation (49) with a blackbody initial spectrum given by equation (13) for f_0.
It is now possible to obtain the light curves using equation (33) for the part where it has reached equilibrium. This is done for a temperature of $kT=0.1$, amplitude of $A=0.1$ and three different angular frequencies given by $\omega=\frac{2\pi}{\sqrt{3}}$, $\omega=2\pi$ and $\omega=2\pi\sqrt{3}$ and is shown in Figure 20.

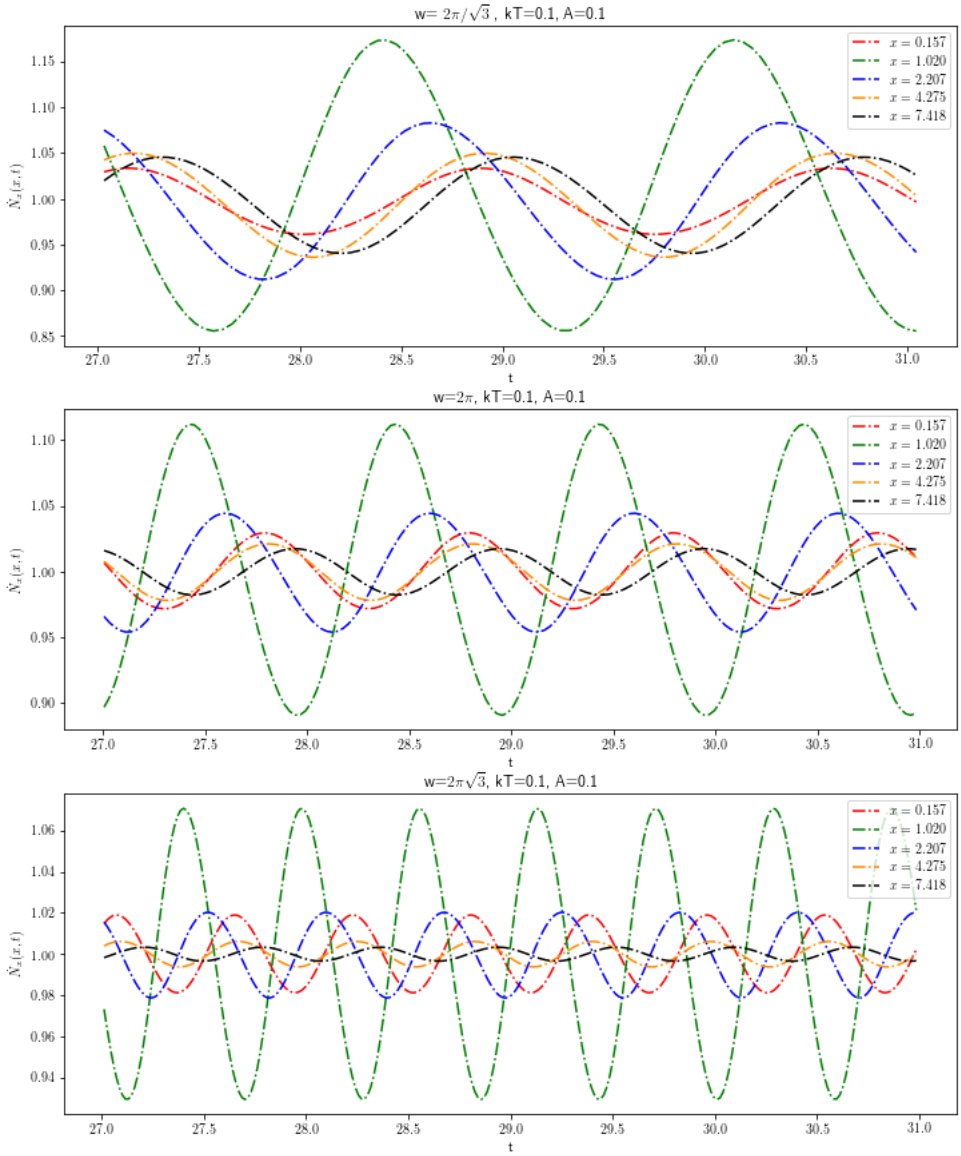

Figure 20: Time-dependent escaping photon energy distribution in units of the injection rate $\dot{N}_0$ for a blackbody initial spectrum with a varying temperature. In the top panel $kT=0.1$, $\tilde{y}=1.0$, $A=0.1$ and $\omega=\frac{2\pi}{\sqrt{3}}$. In the middle panel $kT=0.1$, $\tilde{y}=1.0$,$A=0.1$ and $\omega=2\pi$. In the bottom panel $kT=0.1$, $\tilde{y}=1.0$, $A=0.1$ and $\omega=2\pi\sqrt{3}$. The light curve is selected in the large time range to obtain only the part that has reached equilibrium.

Next, it is possible to study the power spectrum of the light curves by computing the FFT. The results of the power spectra are shown in Figure 21 for the same values used in Figure 20.

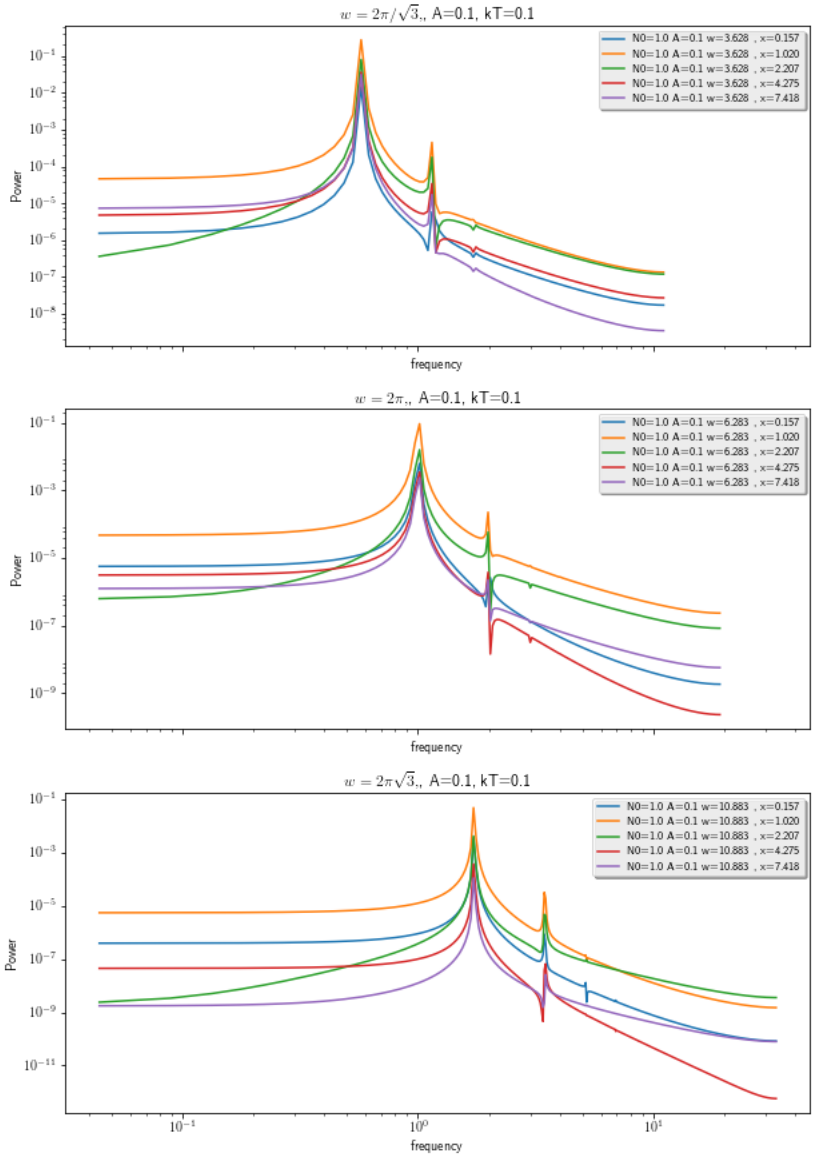

Figure 21: FFT of the time-dependent escaping photon energy distribution light curves in units of the injection rate $\dot{N}_0$ for a blackbody initial spectrum with a varying temperature. In the top panel $kT = 0.1$, $\tilde{y} = 1.0$, $A = 0.1$ and $\omega = \frac{2\pi}{\sqrt{3}}$. In the middle panel $kT = 0.1$, $\tilde{y} = 1.0$,$A = 0.1$ and $\omega = 2\pi$. In the bottom panel $kT = 0.1$, $\tilde{y} = 1.0$, $A = 0.1$ and $\omega = 2\pi\sqrt{3}$. The light curve is selected in the large time range to obtain only the part that has reached equilibrium.

Finally, the spectra can show some useful information on the behaviour of the time-dependent escaping photon distribution when the temperature is varied. As previously mentioned a spectrum refers to the time-dependent escaping photon distribution versus the energy at different values of the time t. A model is made that shows the change of the spectra over time and can be found on the GitLab page from the author. [18] Figure 34 shows the spectrum with a slider over the time where it is set on $t = 16.31[t_{esc}^{-1}]$.

3.8.2. Physical explanation

Figure 20 shows that with increasing angular frequency the amplitude of the light curves decreases. When plotting the light curves for the time-dependent escaping photon distribution without the Comptonisation as done in Figure 36 in Appendix G it is seen that the amplitudes are all the same for different energies but not for different angular frequencies. Therefore it is possible to say that the amplitude change with energy is due to Comptonisation but the amplitude change with angular frequency is not.
The phase lags of the curves for each panel appear to increase with increasing energy for all the curves except the red ones, which have the lowest energy value. A way to check this is to plot the phase lag versus energy at the QPO frequency. This is shown in figure 37 in Appendix H for both the fundamental and second harmonic. It shows that the phase lags increase with increasing energy until they reach a certain energy and then start decreasing again. It is not certain what causes this and can be further investigated.

Figure 21 clearly shows a second harmonic next to the fundamental harmonic in the power spectrum. It also shows a third harmonic next to the second harmonic. The second and third harmonic is caused by the temperature variations since the temperature variations in the light curves do not represent a perfect sine function but is proportional to $\frac{1}{e^{x\frac{kT_e}{kT(1+\sin(\omega t))}}} - 1$.
The place of the peaks of the harmonics in the power spectra move down vertically with increasing energy for every angular frequency. This is caused by the amplitude changes seen in Figure 20. The reason for this is Comptonisation as mentioned earlier.

When changing the time the spectra will move up and down with a wiggle as a result of the oscillation. This effect is best shown by using a slider for the time or making an animation over the time which can clearly show the changes in the spectra. The Python code for the model is avalaible upon request and the animation can be found in the code as well.
When comparing the spectrum of the oscillation in the photon injection rate to the spectrum of the oscillation in the temperature it can be seen that there is a difference between the spectra. Figure 34 in Appendix E shows the difference at one specific time value ($t = 16.31[t_{esc}^{-1}]$) but the dynamical changes between the two are best shown in an animation or by using a slider over the time. This is done in the model and can be accessed upon request.

4. Discussion

There are some points that can be discussed as to why some things were done or why certain results are useful. This discussion is divided into two parts: One that discusses the theoretical model and another that discusses the physics behind it.

4.1. Theoretical model

It was important that the part of the code that would be used multiple times throughout the calculations was fast. This would reduce the time to run the code and to obtain the results. Therefore some adjustments were made in the code.

One of the adjustments that was made is on the Whittaker functions. These are written out into equations instead of importing them from a Python module. Using a self-written routine decreases the runtime of the code and makes it more efficient. The Pochhammer functions inside the Whittaker functions are also written out in the routines, instead of being imported by a Python module for the same reason.
The model uses cache functions to store results in memory. The function stores the calculations in this memory. When a calculation is done a second time with the exact same values the function returns the result from its memory. This decreases the run time of the code.

The time values (t) for the time-dependent escaping photon distribution first contained values between $0.01/t_{esc}$ to $30/t_{esc}$. Here round-off errors in the calculation of the Fast Fourier Transform (FFT) of the light curves of the escaping photon distribution appeared. These round-off errors are the results of rational numbers in the stepsize for the values of the time t. These numbers are 'multiples' of the frequency and cause errors in the calculation. Changing the end value of the time to an pseudo irrational number (irrational up to the computer's precision), e.a. Euler's number, creates an pseudo irrational time-step. Therefore the time-steps are not 'multiples' of the frequency any more and this solves the numerical errors that occurred before.

Since all that is used is a model based on equations and self-entered variables and not on data there are no measurement errors. This does not mean that there are no errors. As previously mentioned, numerical round-off errors do occur in the code and they are caused by the numerical precision of the computer. This happens because there are not enough steps used for the integrations and increasing the number of steps would increase the numerical precision of the computer and therefore give better results. A disadvantage of this is that it would also increase the computation time of the model and therefore it is necessary to consider whether the computational precision is high enough or if it should be increased or decreased.

A similar model to the one created in this report has already been done numerically by Karpouzas [12]. Both models are useful, but since Karpouzas' model is a numerical model and the model created here is an analytical model, there are some differences. For instance, if one wants to study a corona with the electron temperature kT_e and the optical depth τ as a function of the radius. The Python-model created here assumes that these variables are independent of the radius, r. Karpouzas' model has the value of the electron temperature kT_e at the QPO frequency. [12]
Similarly, if one is interested in the oscillations of kT_e induced by the variations of the input spectrum, the model created here is in principle easier to adapt.
The oscillations in the model by Karpouzas [12] have to be harmonic, while the oscillations in the Python-model created can be changed to more complicated oscillations.
A disadvantage of the created Python-model is that the run-time of the model compared to Karpouzas' model [12] is significantly longer due to the analytical calculations instead of numerical ones.

Finally, the Python-model is not a perturbative solution, whereas the model by Karpouzas [12] assumes that all variable terms, like the amplitude in the oscillation, are all small ($A << 1$), while the Python-model is accurate for any amplitude, A.

4.2. Physics

The model that is produced here has some limitations due to assumptions that are made. However, it does include more aspects than other models made by Zeldovich & Sunyeav [22] and Payne [17]. Their solution to the Kompaneets' equation assumes that $\epsilon << kT_e$, and the part that includes electron recoil were ignored. This results in a simplified solution. In reality, this is not the case when photons remain in the cloud long enough to be up-scattered. Therefore the created Python-model does include the recoil effect. [5]
Existing numerical models, for example by Böttcher & Liang [6], often depend on boundary conditions which are not precisely known and therefore the boundary conditions must be assumed. This decreases the computational efficiency of those models and makes them less useful. Therefore the model that is created here merely depends on analytical solutions. [5]

Nonetheless, the model does have some limitations. One of those limitations is that the specific intensity, photon occupation number and source term in the Kompaneets' equation are considered isotropic. Another assumption made is that there is no radiation present in the corona at $t = 0$ and that there is no radiation coming into the corona from the outside. [5] These assumptions are made for simplification and do not resemble reality.

In case of a bremsstrahlung initial spectrum, the initial spectrum initially contains an infinite number of photons at low-energies and this makes it impossible for the spectrum to reach a Wien equilibrium. Therefore the low-energy cut-off at critical energy, x_*, is introduced and result in a finite number of photons in the initial spectrum.[5]
The time-dependent photon energy distribution resulting from the Comptonisation of a bremsstrahlung initial spectrum was done using equation (49) where f_0 is given by equation (12), while in the paper by Becker[5] the equation for the time-dependent photon energy distribution resulting from the Comptonisation of a bremsstrahlung initial spectrum is given by

$$f(x,y) = \frac{32}{\pi} e^{-9y/4} x^{-2} x_*^{-2} e^{-x+x_*)/2} \int_0^\infty e^{-u^2 y} \frac{u \sinh(\pi u)}{(1+4u^2)(9+4u^2)} W_{2,iu}(x) \\ [W_{1,iu}(x_*) - 3W_{0,iu}(x_*) + 6W_{-1,iu}(x_*) - 6W_{-2,iu}(x_*)]\, du + S. \tag{34}$$

This, however, did not result in a different outcome when comparing Figure 4 with Figure 11 since equation (34) is the result of equation (49) for a bremsstrahlung initial spectrum.

The solution for the time-dependent escaping photon distribution assumes that the escape time t_{esc} is constant and that there are initially no photons in the corona. This simplification is done to make the problem less complex.

The model does not contain a variation in the electron temperature and electron number density in the corona, instead, those are assumed constant. When there is a large amount of soft radiation injected into the corona, inverse-Compton cooling of the electrons occurs. It is therefore necessary to implement a temperature variation in the electron temperature in the corona since that aspect is not included in the model created here and the model by Becker [5]. These variations should be dependent on time and position because they are correlated with the hydrodynamics and thermodynamics of the gas.[5]

5. Conclusion

A partly analytic and partly numerical Python model to study the radiative and thermodynamical properties of a corona around a compact object has been created. This model includes the effect of electron recoil. To create the Python-model a closed-form analytic solution to the Kompaneets' Green's function derived by Becker [5] has been used. This solution describes the evolution of an initially mono-energetic radiation spectrum in an infinite medium under the influence of repeated Compton scattering. [5]
The model generates both the light curves and spectra, as well as the power spectra using the escaping photon distribution in units of the injection rate for a blackbody initial spectrum. Here the temperature and photon injection rate from the source can be varied independently to achieve a more realistic model.

Other things the model calculates are the mean photon energy, the inverse-Compton temperature ratio and the photon energy distribution for a mono-energetic, bremsstrahlung and blackbody initial spectrum. The time-dependent escaping photon distribution for a mono-energetic, bremsstrahlung and blackbody initial spectrum in units of the escape time is also calculated by the model.

The spectra, light curves and power spectra from the Python-model can be compared with observational data to understand the processes happening in X-ray binaries. The more accurate the model becomes, the more can be understood about X-ray binaries.

6. Recommendations

The model contains the effect of electron recoil and has either a temperature variation or photon injection rate variation. To create a more realistic model it is advised to combine the temperature oscillation with photon injection rate oscillation. Here the injection rate varies and the outcome at time t of the escaping photon distribution can be used as feedback for the temperature at the next timestep $t + dt$. The escaping photon distribution produced can be used to calculate the temperature change and this value can be combined with the temperature from the previous calculation.

Another aspect that can be added is electron temperature oscillations (the value of kT_e) when the temperature (kT) changes. When an large number of photons is injected into the hot corona the electrons will cool due to inverse-Compton scattering. This will vary the electron temperature and therefore it is necessary to add the electron temperature changes in the model.

Finally, the model might be improved by making it faster. Numerous aspects have been added to the model to make it faster, like writing the Whittaker functions as a full equation instead of using a built-in module from Python. The model also uses cache functions to decrease the run time. However, improvements can always be made and it is therefore advised to look at the code in order to see if it can be made even faster.

7. Self-reflection

The project that I was allowed to do was quite challenging. At the beginning of this internship, the planning was to create a Python-based computer model of the analytical calculations done in the paper by Becker [5]. This required me to read and understand the paper in detail. When first reading it, I had a hard time understanding what was explained and described in the paper. However, this did not stop me and even so encourage me to dig deeper and try to understand the paper. I did this by googling a lot and asking questions to my supervisors. Although I had not understood everything in the paper, I challenged myself to just begin and learn along the way. This way of working helped me very much because I learned more this way. When I got stuck on some things I googled them or asked them to my supervisors. In the beginning, I was struggling with asking some easy things that can be googled or looking at something too long without asking. This is something that I improved during the internship. I learned how to google certain things to get my answers and then if I still could not figure it out ask my supervisor. However, I also learned that I should not wait too long to reach out to them since this would only take time and therefore I would have less time to work on other things or get further with the assignment.

Since I already had experience with programming in Python and I enjoy it very much, I recreated the paper in less than 2 months. This gave me some confidence in the things I was doing and encouraged me to go even further. My supervisors therefore suggested that I should implement the variation in the photon injection rate and the temperature. This was a little more challenging and took me a little longer to figure out. However, I did learn a lot about programming this way. Having already recreated the paper gave me some peace of mind that I did not have to hurry with the second assignment since I already had done enough work for my report. This gave me time to try to understand the second problem about the variations and create a computer model for it. I was motived by the fact that everything went very well and this only motivated me to do more and more and see how much I could get done during this internship. I think that I had a nice balance between working fast and trying to really understand the problem. This means that I did not work too hasty and made a fast and good code, but I also made sure not to work too slow.

What I did learn from the interaction with my supervisors is that when I have a question about something I have to formulate it very clearly or give some more background information. I know exactly what I am talking about but my supervisors do not, and therefore it is necessary to explain what I mean and to clearly formulate what I want to ask. I experienced that sometimes I asked something very vague and a lot of miscommunication occurred due to the fact that I did not formulate my questions correctly.

References

[1] Free-free radio emission from an hii region.

[2] Kapteyn astronomical institute.

[3] X-rays - roentgen radiation.

[4] Binary stars, Nov 2020.

[5] P. A. Becker. Exact solution for the green's function describing time-dependent thermal comptonization. *Monthly Notices of the Royal Astronomical Society*, 343(1):215–240, Jul 2003.

[6] M. Böttcher and E. P. Liang. Comptonization Signatures in the Rapid Aperiodic Variability of Galactic Black Hole Candidates. *The Astrophysical Journal*, 506(1):281–288, October 1998.

[7] Hale Bradt. *Astrophysics processes: the physics of astronomical phenomena.* Cambridge Univ. Press, 2014.

[8] Max Camenzind. *Compact objects in astrophysics: white dwarfs, neutron stars and black holes.* Springer, 2007.

[9] Thierry J.-L. Courvoisier. *High energy astrophysics an introduction.* Springer, 2013.

[10] Matt DeCross, Christopher Williams, Sameer Kallasa, Deeponjit Bose, Josh Silverman, Jimin Khim, and Andrew Hayes. Green's functions in physics, Dec 2020.

[11] Juhan Frank, Andrew R. King, and Derek J. Raine. *Accretion power in astrophysics.* Cambridge Univ. Pr., 1985.

[12] Konstantinos Karpouzas, Mariano Méndez, Evandro M. Ribeiro, Diego Altamirano, Omer Blaes, and Federico García. The Comptonizing medium of the neutron star in 4U 1636 - 53 through its lower kilohertz quasi-periodic oscillations. *Monthly Notices of the Royal Astronomical Society*, 492(1):1399–1415, February 2020.

[13] Kenneth R. Lang. Black body radiation, 2010.

[14] J.D. Myers. X-ray binary stars - introduction, 2014.

[15] Michael A. Nowak, Brian A. Vaughan, Jörn Wilms, James B. Dove, and Mitchell C. Begelman. Rossi X-Ray Timing Explorer Observation of Cygnus X-1. II. Timing Analysis. *The Astrophysical Journal*, 510(2):874–891, January 1999.

[16] Michael A. Nowak, Brian A. Vaughan, Jorn Wilms, James B. Dove, and Mitchell C. Begelman. Rossi x-ray timing ExplorerObservation of cygnus x-1. II. timing analysis. *The Astrophysical Journal*, 510(2):874–891, jan 1999.

[17] D. G. Payne. Time-dependent comptonization : X-ray reverberations. *The Astrophysical Journal*, 237:951–963, May 1980.

[18] J. Roomer. An analytic model to study the radiative and thermodynamic properties of a corona around a compact object. `https://gitlab.astro.rug.nl/roomer/an-analytic-model-to-study-the-radiative-and-thermodynamical-properties-of-a-corona-arc` `git`, 2022.

[19] George B. Rybicki and Alan P. Lightman. *Radiative processes in astrophysics.* WILEY-VCH, 2004.

[20] Mario Vietri. *Foundations of high-energy astrophysics.* University of Chicago, 2008.

[21] Michael D. Wright. Microbeam radiosurgery: An industrial perspective. *Physica Medica*, 31(6):601 – 606, 2015. Radiation Therapy with Synchrotron Radiation: Achievements and Challenges.

[22] Ya. B. Zeldovich and R. A. Sunyaev. The Interaction of Matter and Radiation in a Hot-Model Universe. *Astrophysics and Space Science*, 4(3):301–316, July 1969.

A. Background theory

A.1. Blackbody radiation

Blackbody radiation is used widely in astrophysics. It emerges when photons are scattered many times in an optically thick region and hence matter and radiation are in thermodynamical equilibrium. The specific intensity of blackbody radiation is given by

$$B_\nu(T) = \frac{2h\nu^3}{c^2}\frac{1}{e^{h\nu/kT}-1}, \tag{35}$$

$$B_E(T) = \frac{2E^3}{c^2h^2}\frac{1}{e^{E/kT}-1}, \tag{36}$$

$$B_x(T) = \frac{2x^3}{c^2h^2}(kT_e)^3\frac{1}{e^{x\frac{kT_e}{kT}}-1}. \tag{37}$$

Where $E = h\nu$ and $x = E/kT_e$. Here T is the temperature, h the Planck constant, ν the frequency, c the speed of light, k the Boltzmann constant, E the energy and x the dimensionless energy in units of the electron temperature kT_e. [7, 19] Equation (34) is also known as the Planck radiation law or Planck function. An example is plotted in Figure 22.

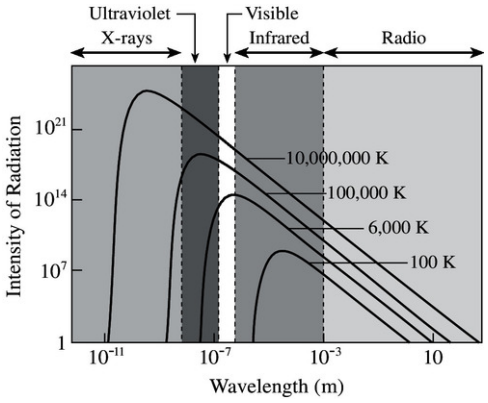

Figure 22: Blackbody radiation intensity as a function of wavelength for different values of the temperature. [13]

A.2. Wien's law

When the Compton y-parameter $y \gg 1$, saturation of inverse-Compton scattering occurs and a Wien spectrum is produced. A property of the blackbody radiation is that when $h\nu \gg kT$ the Wien's law is obtained: [19]

$$I_\nu(T) = \frac{2h\nu^3}{c^2}e^{\frac{-h\nu}{kT}}, \tag{38}$$

$$I_x(T) = \frac{2x^3}{h^2c^2}(kT_e)^3 e^{\frac{-xkT_e}{kT}}. \tag{39}$$

A.3. Comptonisation

Comptonisation is the process of electron recoil as a result of an interaction with a photon. [20] When a photon collides with an electron at rest and gives that electron energy it is called Compton scattering. Figure 23 gives an illustration of the process.

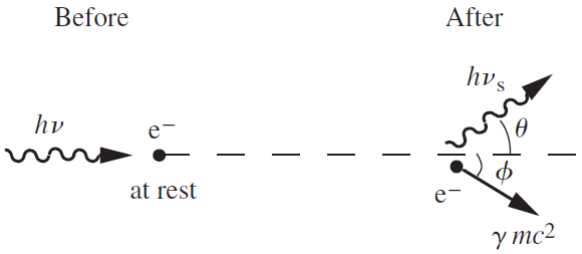

Figure 23: Compton scattering. [7]

Furthermore, when the opposite occurs and the electrons will give the photon energy it is called inverse-Compton scattering. Figure 24 shows the effect of inverse-Compton scattering.

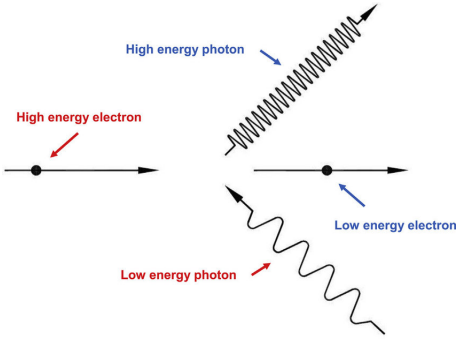

Figure 24: Inverse Compton scattering. [21]

A.4. Binary systems

Binary systems consist of two stars which orbit around a common centre of mass. In binary systems one of the components is a compact object. The compact object can be three things: a black hole, a neutron star or a white dwarf. [14] When the stars are close enough together, one of the stars will strip matter from its companion. There are two main reasons this matter transfer can occur:

1. One of the stars in the system increases in size due to its stellar evolution and it will fill its Roche lobe. Matter will then start to flow to the companion star through the inner Lagrangian point due to its gravitational pull. This is called Roche lobe overflow. Figure 25 shows the process.

2. One of the stars blows out its exterior in the form of stellar wind and the companion star will capture the material ejected. This is called stellar wind accretion. Figure 26 shows the process.

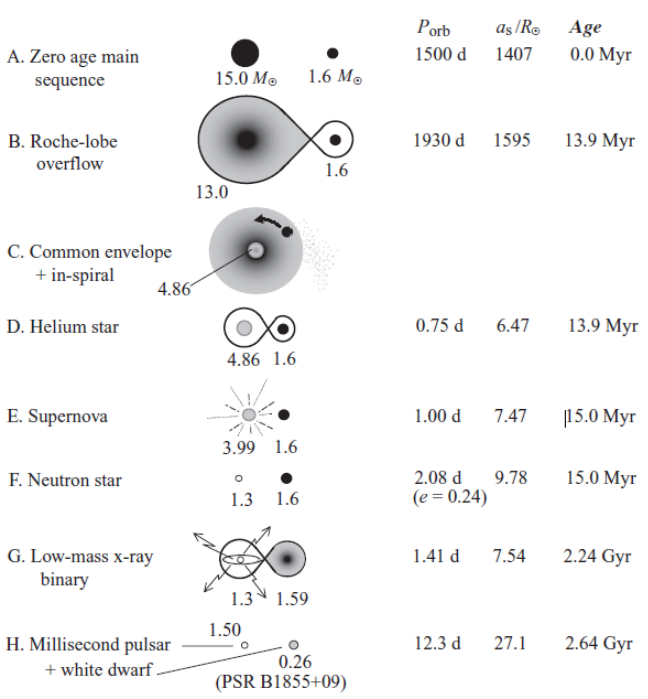

Figure 25: Evolution of a binary system that leads to a LMXB. [7]

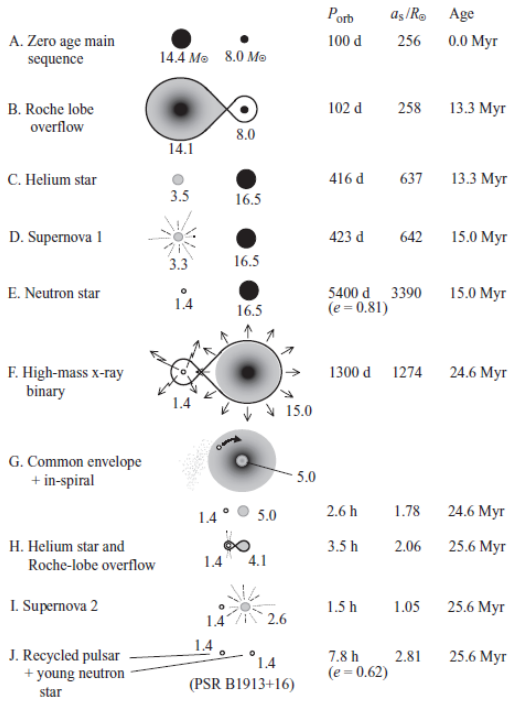

Figure 26: Evolution of a binary system that leads to a HMXB. [7]

A special case of binary systems are X-ray binaries. These systems emit X-ray radiation and consist of a normal star and a neutron star. [4, 14] When the companion star has a mass that is lower than the neutron star in the system the mass transfer will be as described in the first case. These systems are called Low Mass X-ray Binaries (LMXB). When the companion star has a higher mass then that of the neutron star the mass transfer occurs through stellar winds as described in the second case. These are High Mass X-ray Binaries (HMXB). [8] Figure 27 gives a schematic overview of the difference between the two systems.

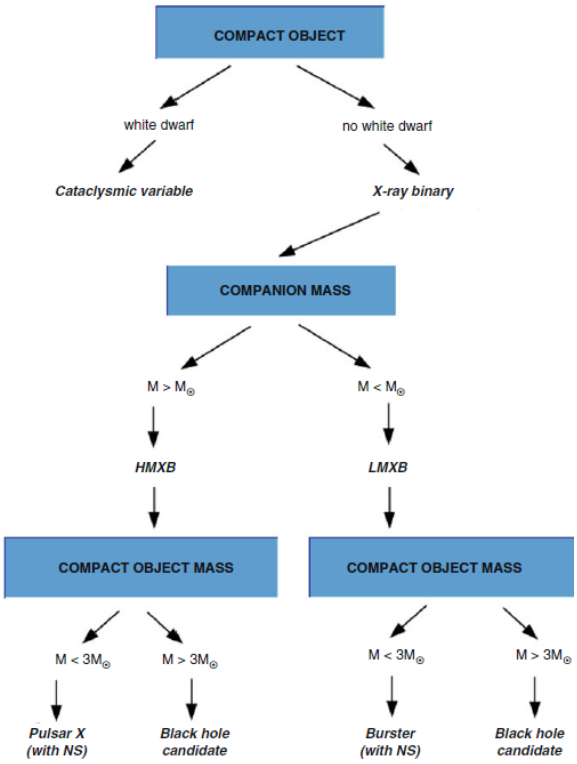

Figure 27: Types of X-ray binaries. [9]

LMXB are considered the older population of binaries since the companion stars are less massive than the Sun and therefore have not evolved and died yet. The companion star will fill its Roche lobe and therefore matter will transfer through the inner Lagrangian point to the neutron star. The matter that transfers onto the neutron star has a high angular momentum and therefore it is not possible for the matter to fall directly onto the neutron star. It will fall into orbit around it and form an accretion disc. The process is shown in Figure 28.

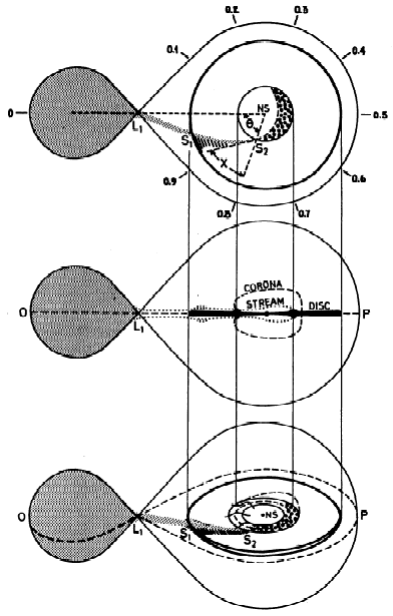

Figure 28: Roche lobe overflow. Taken from [11]

When matter moves toward the centre of the disc in a circular orbit it loses gravitational energy more rapidly and the temperature of the disc increases. X-ray emission is then the process that cools it down. [9] Heating of the disc creates a corona above and below the disc as seen in Figure 28. This corona Comptonises photons coming from the disc and creates a hard component in the observed X-ray emission spectrum. [8]
In a big fraction of the LMXB hydrogen and helium ignite in powerful nuclear fusion reactions and creates bursts of X-ray radiation. These are called X-ray bursters. The spectra of these bursts are very similar to that of a blackbody spectrum. [9]
Neutron stars in LMXB spin very rapidly due to the accretion of matter. Around 1996 researchers found variations in the observed X-ray spectra which were almost periodic with frequencies around 1000 Hertz. These oscillations are called Kilohertz Quasi-Periodic Oscillations or kHz QPOs. The origin of the QPOs and why they have specific frequencies is currently unknown. [8]

Hard X-rays are the photons with higher energies, while soft X-rays have lower energies and thus a longer wavelength. [3] Soft photons in the corona are produced when hard radiation from the corona falls in the accretion disc and is reflected or thermalized. The photons then enter the corona again and Compton cool the plasma.
Hard photons undergo more scatterings in the corona than soft photons and are therefore delayed with respect to the soft photons. This delay can be expressed as time and phase lags, where the phase lag is the phase of the averaged cross power spectrum and the time lag is the time delay between the photons. [16]

A.5. Kompaneets' equation

The Kompaneets' equation describes the spectral modification of a photon distribution as it moves through a hot electron population.[19] It is given by

$$\frac{1}{n_e \sigma_T c}\frac{\partial n}{\partial t} = \left(\frac{kT}{mc^2}\right)\frac{1}{x^2}\frac{\partial}{\partial x}\left[x^2\left(n' + n + n^2\right)\right]. \tag{40}$$

Here n' is the diffusion along the x-axis, n is the cooling of the photon population as the photons scatter on electrons that take part in the energy recoil and n^2 is the stimulated reactions. n_e is the electron number density, σ_T the Thomson cross section, c the speeds of light, k the Boltzmann constant, T the electron temperature, t the time and x the energy given by [9]

$$x = \frac{E}{kT_e}. \tag{41}$$

This equation assumes that photons scatter off non-relativistic electrons and therefore the fractional energy transfer for each scattering is small. [19]

The Compton y-parameter is given by

$$y = \frac{kT_e}{m_e c^2}\tau_T, \tag{42}$$

where τ_T is the optical depth. When $y \ll 1$ the spectrum is a modified blackbody. While when $y \gg 1$ there is saturated Comptonisation. For cases between those values the Kompaneets' equation is required. [19]

A.6. Green's function

Green's functions are used to solve complicated differential equations. The definition of the Green's function is as follows: the inverse of an arbitrary linear differential operator L. [10]

Here a differential equation of the form

$$\frac{d^2 f(x)}{dx^2} + x^2 f(x) = 0, \tag{43}$$

will lead to the differential operator L:

$$\left(\frac{d^2}{dx^2} + x^2\right) f(x) = 0 \Longrightarrow Lf(x) = 0. \tag{44}$$

The Green's function is then defined to be

$$G(x, y) \sim L^{-1} \tag{45}$$

and thus

$$LG(x, y) = \delta(x - y). \tag{46}$$

In the end the differential equation can be solved by using

$$Lf(x) = g(x), \tag{47}$$

where $g(x)$ is the response of the differential equation. The solution to the differential equation is then [10]

$$f(x) = G(x, y)g(x). \tag{48}$$

The solution for the distribution function $f(x, y)$ with an initial spectrum $f_0(x)$ and initial energy x_0 using the Green function is given by [5]

$$f(x, y) = \int_0^\infty x_0^2 f_0(x_0) G(x, x_0, y) dx_0. \tag{49}$$

B. Flowchart of Python code

B.1. Flowchart for recreating graphs from Becker [5]

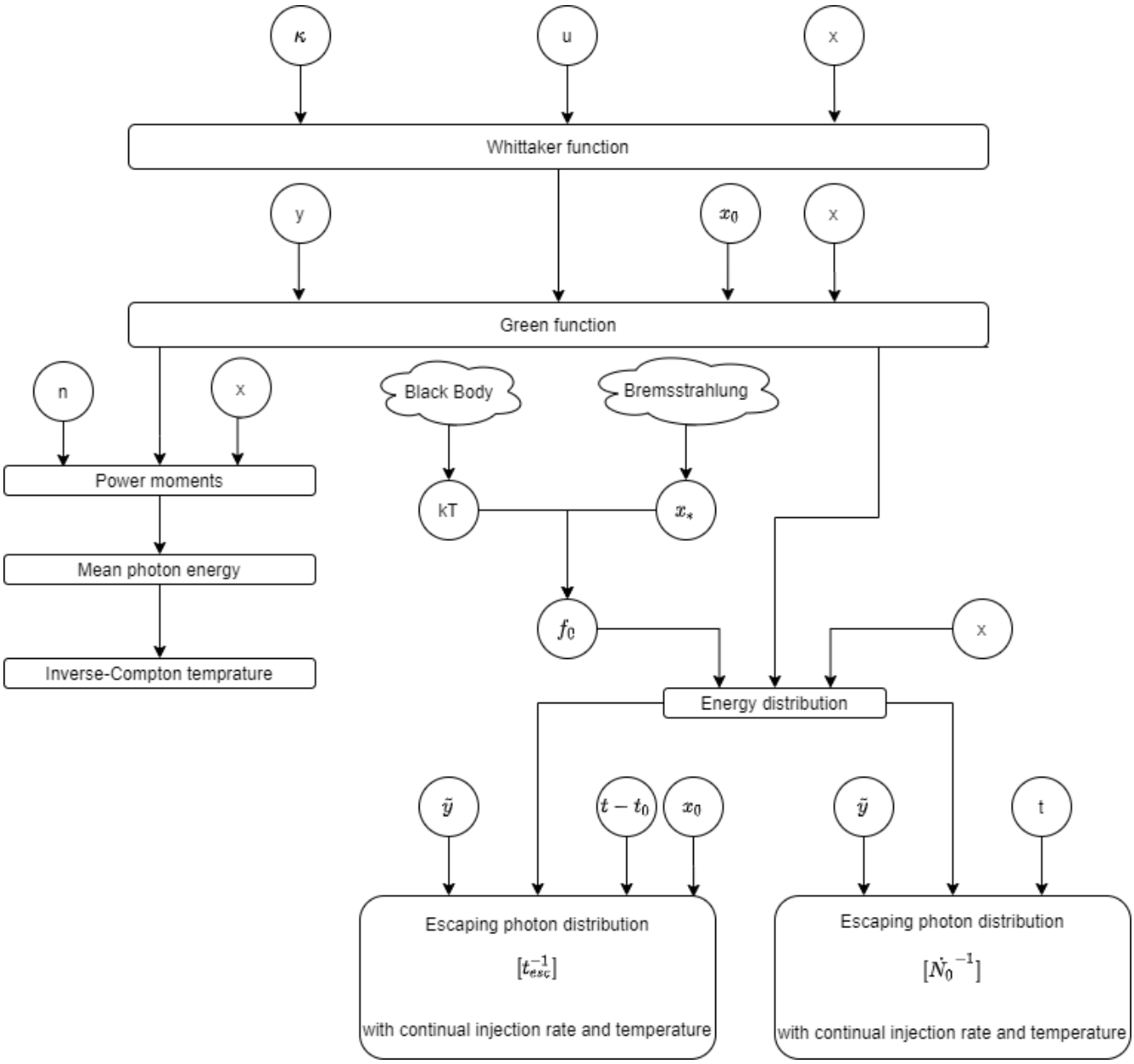

Figure 29: Flowchart of Python code for recreating the graphs for the paper by Becker [5].

B.2. Flowchart for the code to obtain the time-dependent escaping photon distribution with varying injection rate or temperature

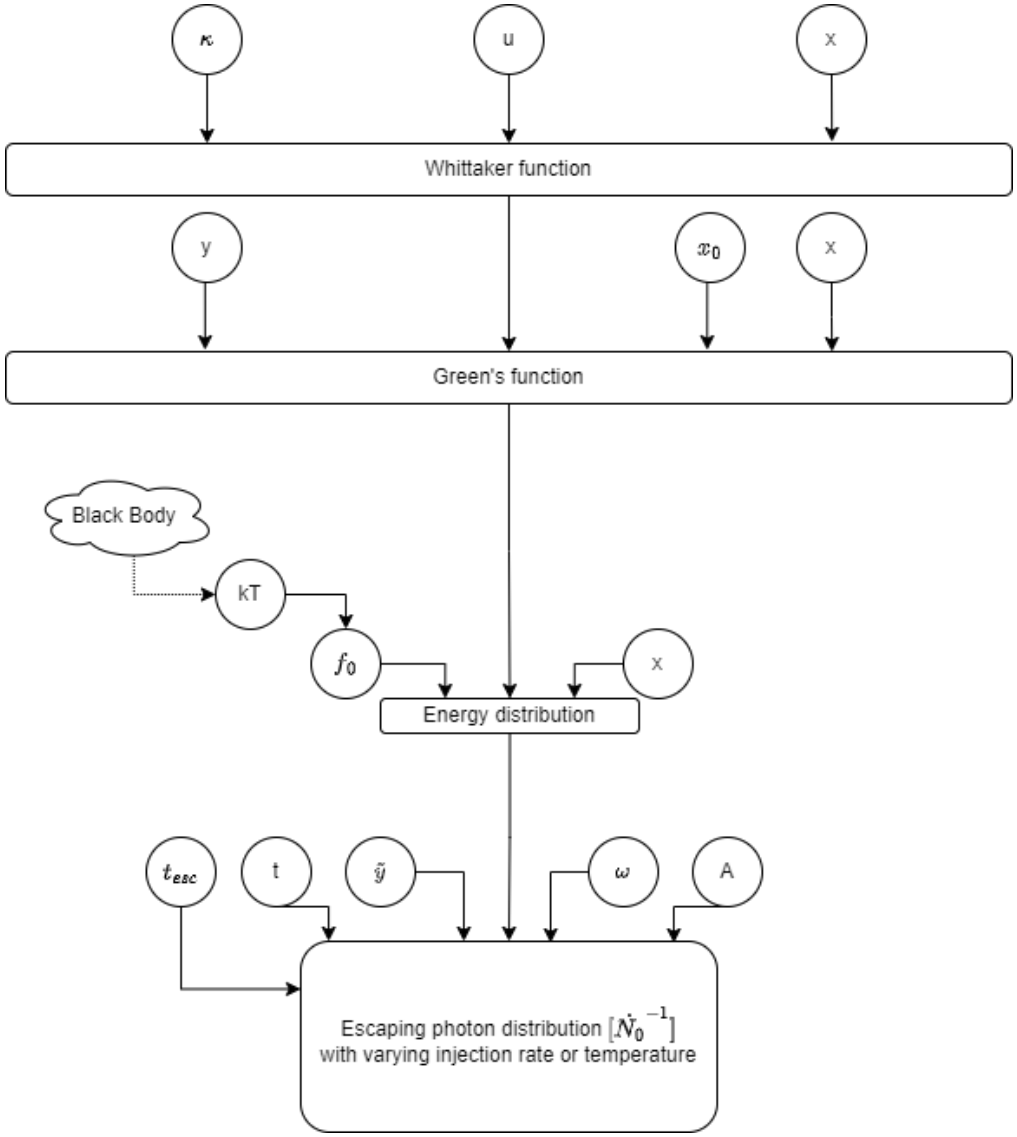

Figure 30: Flowchart of the Python code for the code that creates the time-dependent escaping photon distribution with a varying injection rate or varying temperature.

C. Normalisation condition of the Green's function

Table 1: Second power moment for the Green's function as a check to the normalisation condition given by equation (8) for different values of the initial energy x_0 and Compton y-parameter.

x_0	y	Moment	calc. time (s)
0.010	0.001	1.00365530	0.066
0.010	0.200	0.99990596	0.041
0.010	1.600	0.99993483	0.038
0.010	3.000	0.99996932	0.038
0.100	0.001	1.00086485	0.050
0.100	0.200	0.99997115	0.043
0.100	1.600	0.99997128	0.038
0.100	3.000	0.99997135	0.038
0.500	0.001	1.00007973	0.050
0.500	0.200	0.99997142	0.042
0.500	1.600	0.99997136	0.038
0.500	3.000	0.99997136	0.038
1.00	0.001	0.99992700	0.052
1.00	0.200	0.99997134	0.043
1.00	1.600	0.99997136	0.038
1.00	3.000	0.99997136	0.038
3.00	0.001	0.99998992	0.052
3.00	0.200	0.99997136	0.044
3.00	1.600	0.99997136	0.039
3.00	3.000	0.99997136	0.038
5.00	0.001	0.99997972	0.050
5.00	0.200	0.99997136	0.042
5.00	1.600	0.99997136	0.039
5.00	3.000	0.99997136	0.038

D. Light curves for the time-dependent escaping photon distribution with varying injection rate

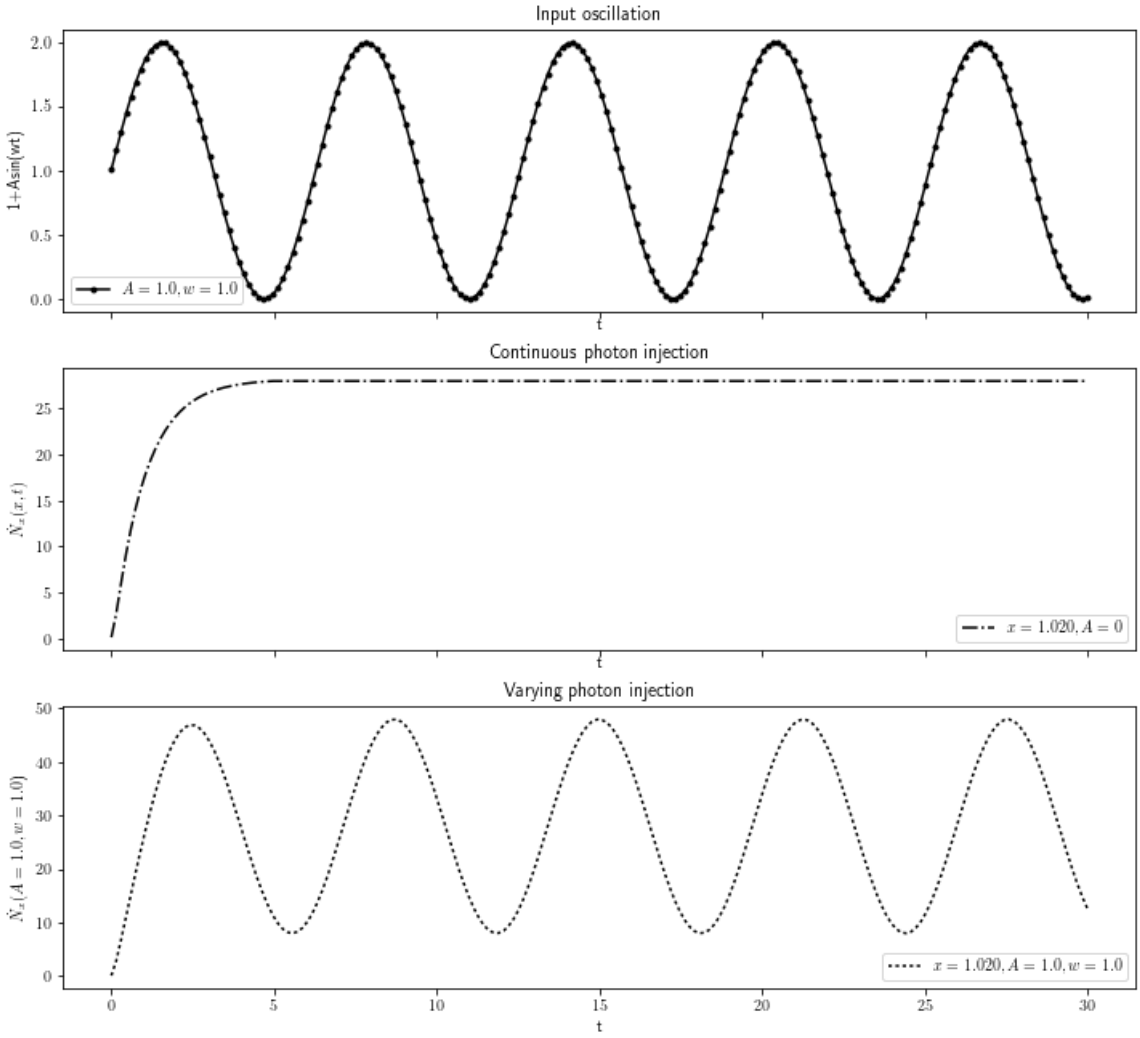

Figure 31: Top panel: Sine function $1 + A\sin(\omega t)$ where $\omega = 1.0$ and $A = 1.0$. Middle panel: Time-dependent escaping photon energy distribution in units of the injection rate $\dot{N}_0$ for a blackbody initial spectrum with continuous injection rate $\dot{N}_0$. Bottom panel: Time-dependent escaping photon energy distribution in units of the injection rate $\dot{N}_0$ for a blackbody initial spectrum with varying injection rate $\dot{N}_0$ (equation (31)). The blackbody temperature in units of the electron temperature, kT, and the mean value of the Compton y-parameter, $\tilde{y}$, are set to the value of 1.

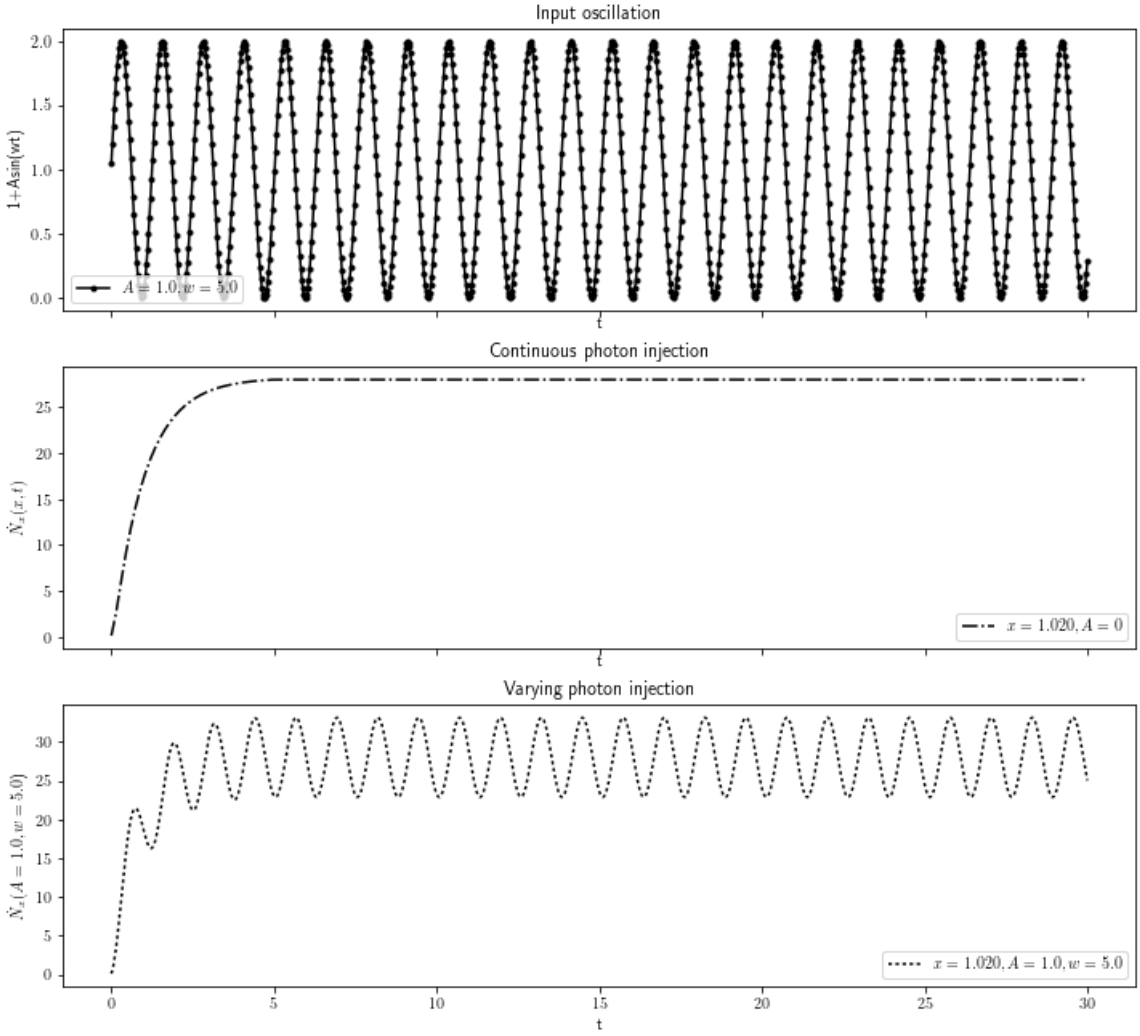

Figure 32: Top panel: Sine function $1 + Asin(\omega t)$ where $\omega = 5.0$ and $A = 1.0$. Middle panel: Time-dependent escaping photon energy distribution in units of the injection rate $\dot{N}_0$ for a blackbody initial spectrum with continuous injection rate $\dot{N}_0$. Bottom panel: Time-dependent escaping photon energy distribution in units of the injection rate $\dot{N}_0$ for a blackbody initial spectrum with varying injection rate $\dot{N}_0$ (equation (31)). The blackbody temperature in units of the electron temperature, kT, and the mean value of the Compton y-parameter, $\tilde{y}$, are set to the value of 1.

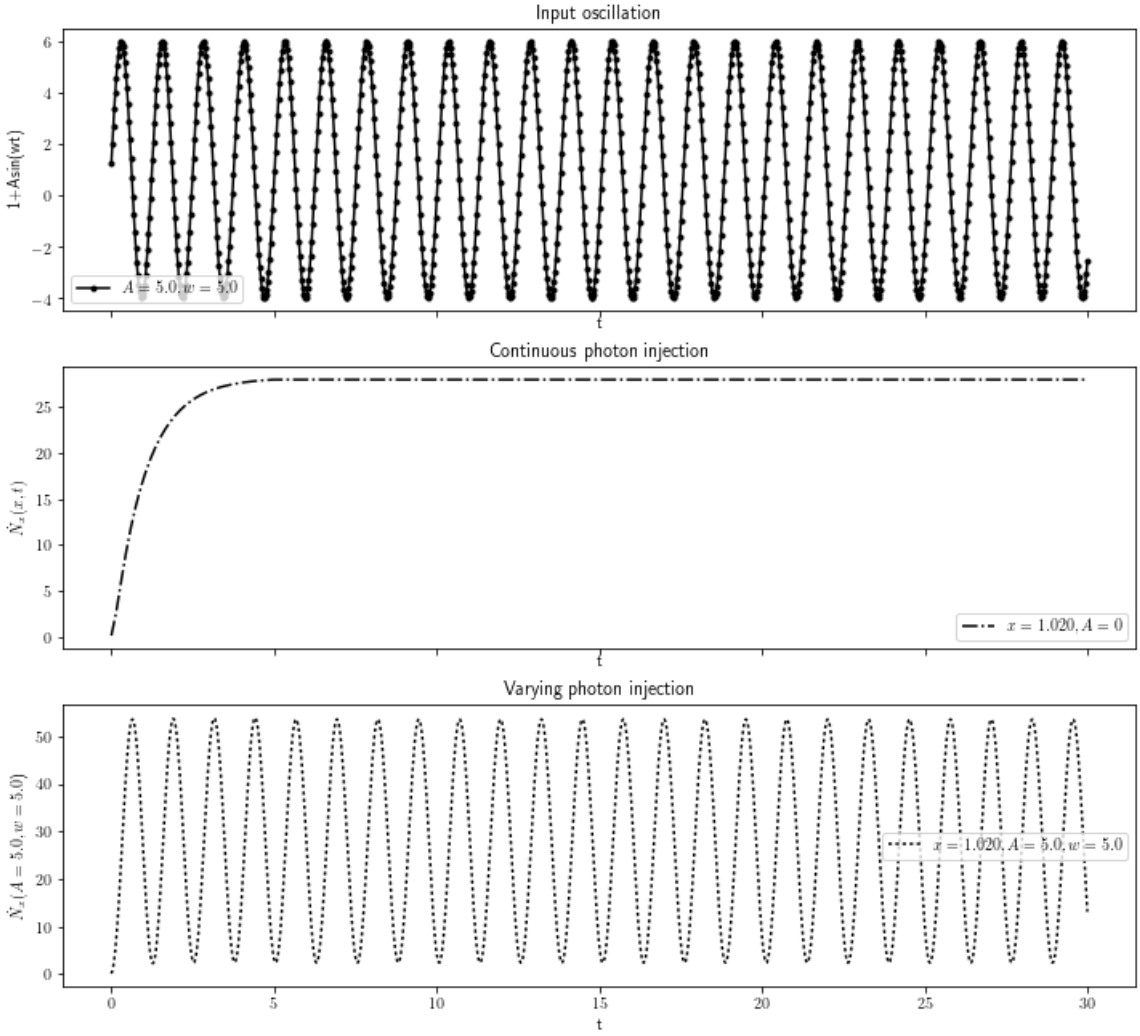

Figure 33: Top panel: Sine function $1 + A\sin(\omega t)$ where $\omega = 5.0$ and $A = 5.0$. Middle panel: Time-dependent escaping photon energy distribution in units of the injection rate $\dot{N}_0$ for a blackbody initial spectrum with continuous injection rate $\dot{N}_0$. Bottom panel: Time-dependent escaping photon energy distribution in units of the injection rate $\dot{N}_0$ for a blackbody initial spectrum with varying injection rate $\dot{N}_0$ (equation (31)). The blackbody temperature in units of the electron temperature, kT, and the mean value of the Compton y-parameter, $\tilde{y}$, are set to the value of 1.

E. Time-dependent escaping photon distribution for a varying injection rate and temperature at time $t = 16.31[t_{esc}^{-1}]$

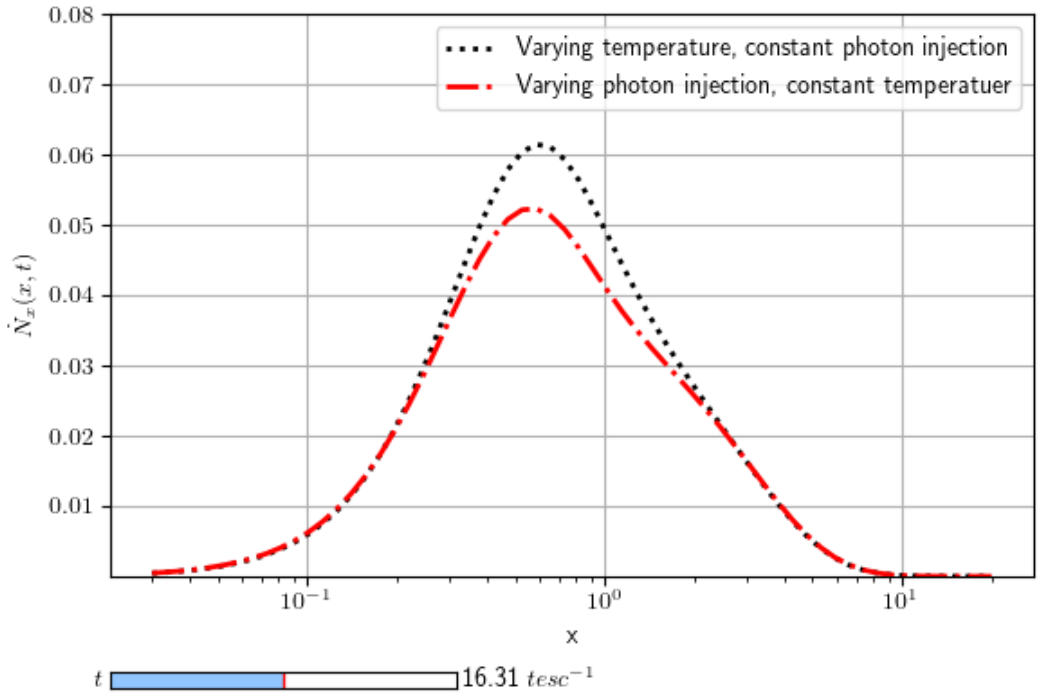

Figure 34: Time-dependent escaping photon energy distribution in units of the injection rate $\dot{N}_0$ for a blackbody initial spectrum with a varying injection rate (red curve) and varying blackbody temperature (black curve). Here the angular frequency $\omega = 2\pi$, the amplitude $A = 0.1$ and the temperature $kT = 0.1$.

F. Phase lags versus energy for a varying photon injection rate

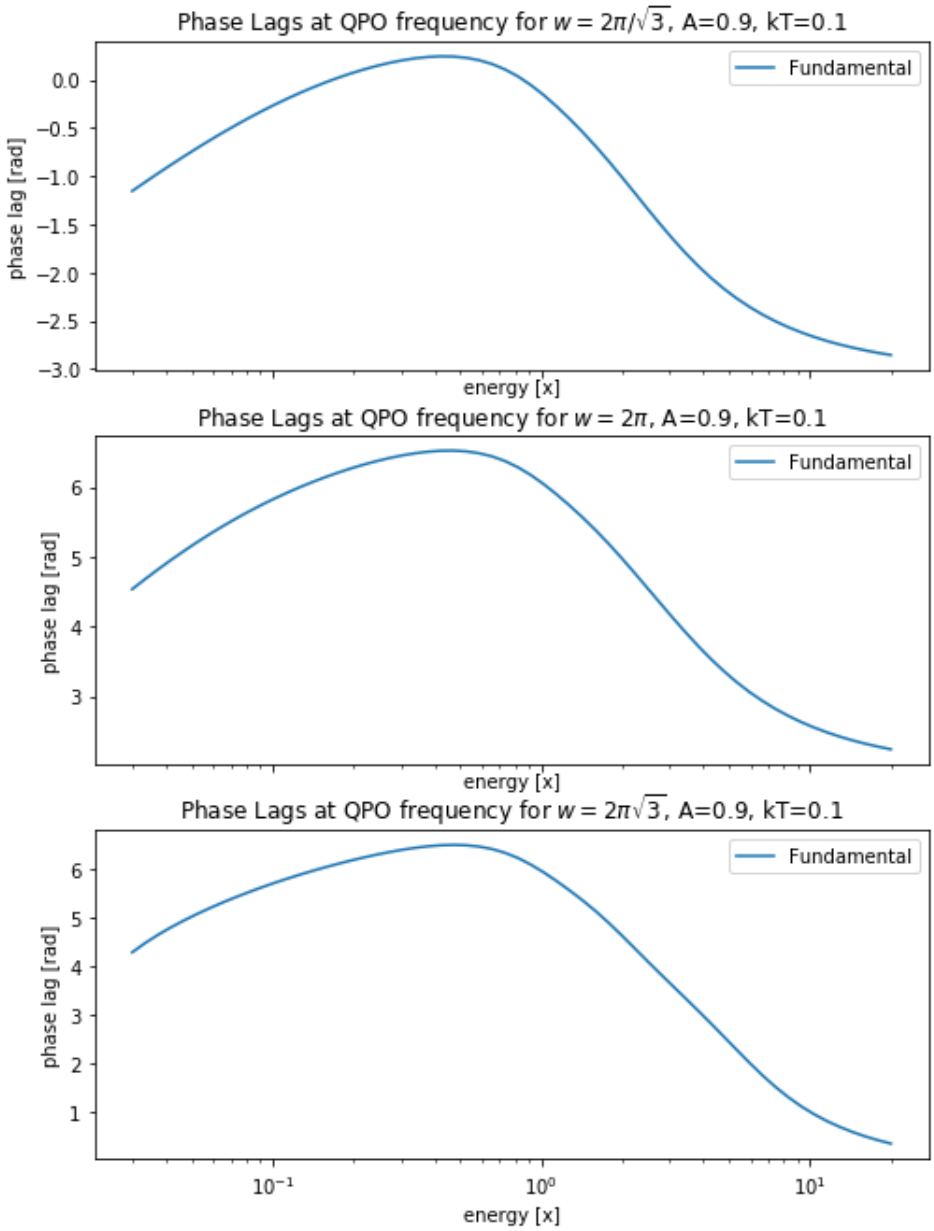

Figure 35: Phase lags between the time-dependent escaping photon energy distributions in units of the injection rate $\dot{N}_0$ for a blackbody initial spectrum with a varying photon injection rate. The blue curve indicates the fundamental harmonic. In the top panel: $\omega = \frac{2\pi}{\sqrt{3}}$, middle panel: $\omega = 2\pi$ and in the bottom panel: $\omega = 2\pi\sqrt{3}$. The amplitude and temperature are given by $A = 0.9$ and $kT = 0.1$ respectively.

G. Light curves for a varying temperature without Comptonisation

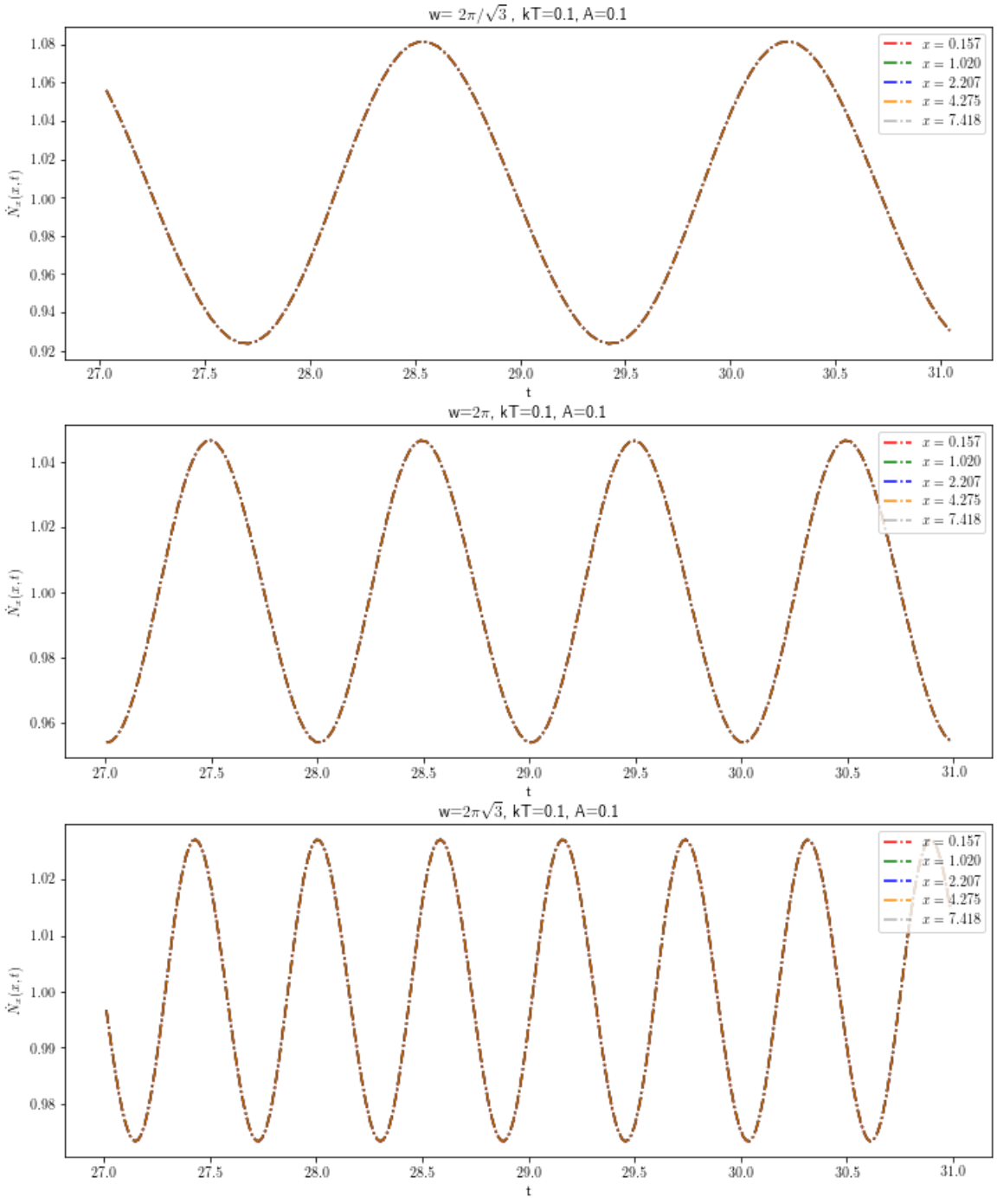

Figure 36: Time-dependent escaping photon energy distribution in units of the injection rate $\dot{N}_0$ for a blackbody initial spectrum with a varying temperature without Comptonisation. In the top panel $kT = 0.1$, $\tilde{y} = 1.0$, $A = 0.1$ and $\omega = \frac{2\pi}{\sqrt{3}}$. In the middle panel $kT = 0.1$, $\tilde{y} = 1.0$,$A = 0.1$ and $\omega = 2\pi$. In the bottom panel $kT = 0.1$, $\tilde{y} = 1.0$, $A = 0.1$ and $\omega = 2\pi\sqrt{3}$. The light curve is selected in the large time range to obtain only the part that has reached equilibrium.

H. Phase lags versus energy for a varying blackbody temperature

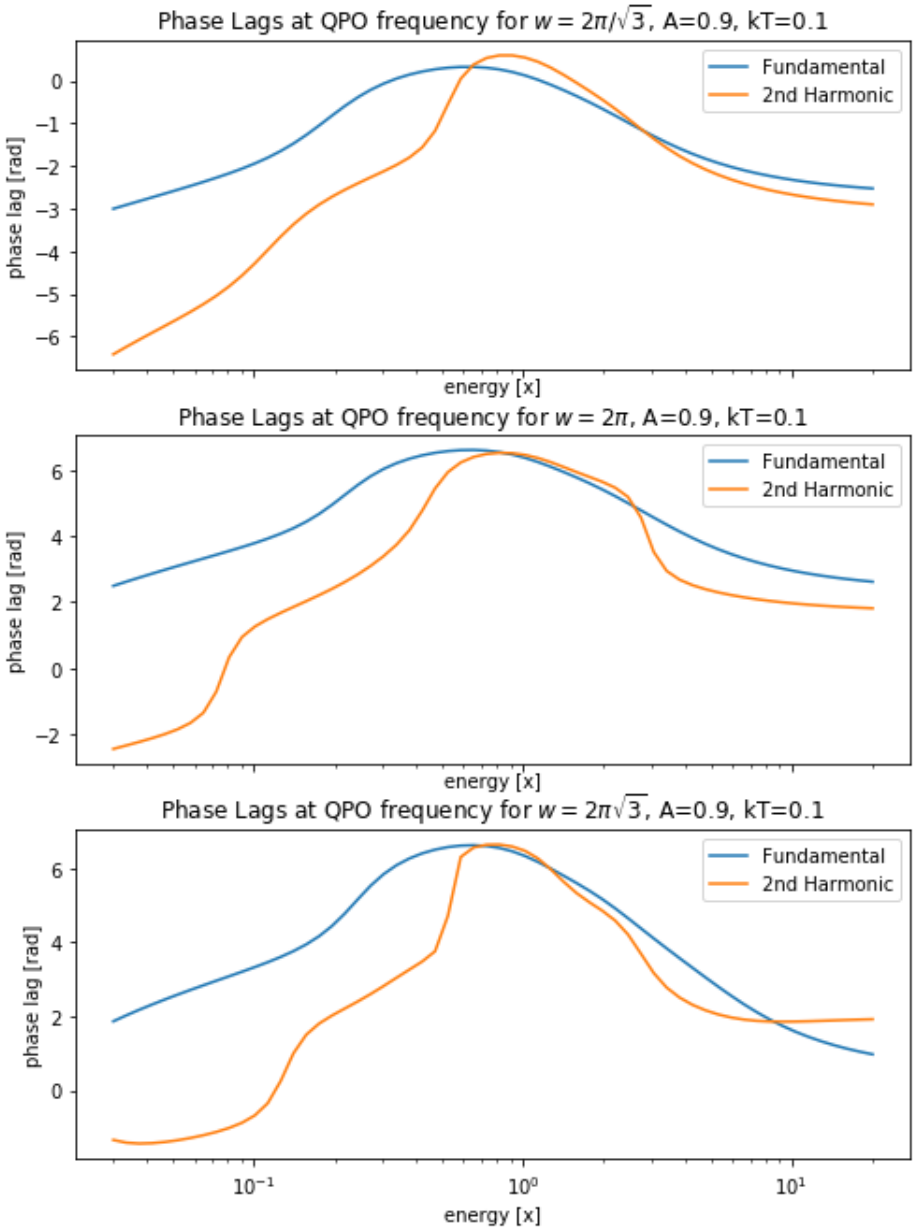

Figure 37: Phase lags between the time-dependent escaping photon energy distributions in units of the injection rate $\dot{N}_0$ for a blackbody initial spectrum with a varying temperature. Here the blue curve indicates the fundamental harmonic and the orange curve the second harmonic. In the top panel: $\omega = \frac{2\pi}{\sqrt{3}}$, middle panel: $\omega = 2\pi$ and in the bottom panel: $\omega = 2\pi\sqrt{3}$. The amplitude and temperature are given by $A = 0.9$ and $kT = 0.1$ respectively.